Transcription of a centromere-enriched retroelement and local retention of its RNA are significant features of the CENP-A chromatin landscape

Santinello B[1], Sun R[1*], Amjad A[1*], Hoyt SJ[1*], Ouyang L[1], Courret C[2], Drennan R[1], Leo L[1,3,4], Larracuente AM[2], Core, L[1,5], O'Neill RJ[1,5,6], Mellone BG[1,5#]

*Equal contributors

#Corresponding author: Barbara.Mellone@uconn.edu

1. Department of Molecular and Cell Biology, University of Connecticut, Storrs, CT, US
2. Department of Biology, University of Rochester, Rochester, NY, US
3. Dipartimento di Biologia e Biotecnologie Charles Darwin, Sapienza University of Rome, 00185 Rome, Italy
4. Present address: RNA editing Lab, Onco-Haematology Department, Genetics and Epigenetics of Pediatric Cancers, Bambino Gesù Children Hospital, IRCCS, 00146 Rome, Italy
5. Institute for Systems Genomics, University of Connecticut, Storrs CT, US
6. Department of Genetics and Genome Sciences, UConn Health, Farmington, CT, US

Abstract

Centromeres depend on chromatin containing the conserved histone H3 variant CENP-A for function and inheritance, while the role of centromeric DNA repeats remains unclear. Retroelements are prevalent at centromeres across taxa and represent a potential mechanism for promoting transcription to aid in CENP-A incorporation or for generating RNA transcripts to maintain centromere integrity. Here, we probe into the transcription and RNA localization of the centromere-enriched retroelement *G2/Jockey-3* (hereafter referred to as *Jockey-3*) in *Drosophila melanogaster*, currently the only *in vivo* model with assembled centromeres. We find that *Jockey-3* is a major component of the centromeric transcriptome and produces RNAs that localize to centromeres in metaphase. Leveraging the polymorphism of *Jockey-3* and a *de novo* centromere system, we show that these RNAs remain associated with their cognate DNA sequences in *cis*, suggesting they are unlikely to perform a sequence-specific function at all centromeres. We show that *Jockey-3* transcription is positively correlated with the presence of CENP-A, and that recent *Jockey-3* transposition events have occurred preferentially at CENP-A-containing chromatin. We propose that *Jockey-3* contributes to the epigenetic maintenance of centromeres by promoting chromatin transcription, while inserting preferentially within these regions, selfishly ensuring its continued expression and transmission. Given the conservation of retroelements as centromere components through evolution, our findings have broad implications in understanding this association in other species.

Introduction

Genome partitioning during cell division is dependent on specialized chromosomal structures known as centromeres, which mediate kinetochore assembly. This process is crucial for establishing robust connections between chromosomes and spindle microtubules, essential for the precise segregation of chromosomes. Centromeric chromatin is marked by the presence of nucleosomes containing the histone H3 variant CENP-A (also known as Cid *Drosophila*)(1, 2), which initiates the recruitment of additional centromeric and kinetochore proteins (3). Centromeres are paradoxical in that they play a highly conserved function across eukaryotes yet are amongst the most rapidly evolving regions of genomes. Centromeres are also dynamic – they can reposition in

44 individuals (neocentromeres)(4) and become fixed in a population (evolutionary new centromeres)(5). Despite
45 being able to reposition, centromeres are typically associated with large highly repetitive sequences whose role
46 in centromere identity remains elusive.

47 Transcripts emanating from centromeres have been observed in a myriad of systems, including budding
48 yeast (6, 7), human cells (8-11), frog egg extracts (12, 13), maize (14), and marsupials (15). Transcription at
49 centromeres has been shown to be coupled to *de novo* centromere formation (16) and neocentromere
50 formation in humans (17-19). In addition, centromeric transcription is critical for programmed histone exchange
51 in *S. pombe* (20), for the stabilization of newly formed CENP-A nucleosomes in *Drosophila* cells (21), and for
52 Human Artificial Chromosome formation (22). These studies suggest that centromeric DNA may contribute to
53 centromere identity through its ability to be transcribed. Other studies have also implicated a role for
54 centromere-derived transcripts as noncoding RNAs important for centromere integrity (8, 9, 12, 14, 15). Indeed,
55 in some cases centromeric transcripts have been detected associated with centromeric proteins (9, 12, 13),
56 suggesting a role beyond being a byproduct of transcription. However, whether the interaction with centromere
57 proteins is sequence-specific remains unresolved. Furthermore, both the functional impact of these RNAs, as
58 well as the extent of their prevalence across different systems, are still not fully understood.

59 Consistent with the existence of centromeric transcripts, elongating RNA polymerase II accumulates at
60 mitotic centromeres in *Drosophila* S2 cells (21, 23) and nascent transcription can be detected at the centromere
61 of *Drosophila* S2 cells in mitosis and G1 (21). However, the RNA products of such centromeric transcription in
62 *Drosophila* are unknown. A previous study analyzed the role of a non-coding RNA produced by a satellite of the
63 1.688 family, showing that its depletion affects accurate chromosome segregation and centromere integrity
64 (23). However, the largest block of this satellite is located within pericentric heterochromatin on the X (24) and
65 its RNA product does not localize to centromeres (21). Therefore, its contributions to centromere segregation
66 accuracy might be unrelated to centromeric defects.

67 The centromeres of *Drosophila melanogaster* have been recently annotated (24), providing a unique
68 opportunity to directly analyze transcripts associated with centromeres. *Drosophila* has five chromosomes (X; Y;
69 2; 3; and 4), each harboring a unique centromere differing in repeat composition and organization. The
70 centromeres are composed of islands of complex repeats enriched in retroelements embedded in large arrays of
71 simple satellites. CENP-A occupies primarily the islands, which are between 101-171-kb, extending only partially
72 to the flanking satellites. All of the repeats present at *Drosophila* centromeres are also present elsewhere in the
73 genome, yet a subset of retroelements are enriched at centromeres (24). Only one element, the non-LTR
74 retroelement *G2/Jockey-3* (henceforth *Jockey-3*), is shared between all centromeres and is conserved at the
75 centromeres of *D. simulans*, a species that diverged from *D. melanogaster* 2.5 million years ago (25) and that
76 displays highly divergent centromeric satellites (26, 27). Retroelements are conserved centromere-associated
77 elements across taxa. In plants, these elements have been proposed to help maintain centromere size and
78 increase the repeat content of neocentromeres (28). Additionally, retroelements could contribute to
79 centromere function in two ways: either by facilitating localized transcription thought to promote CENP-A
80 incorporation (16, 21, 29-33) or by generating transcripts with non-coding roles in maintaining centromere
81 integrity as postulated for other repeats (9, 12, 13, 34). Whether retroelements play such roles remains
82 unknown.

83 Here, we investigate the expression and RNA localization of the conserved centromere-enriched
84 retroelement *Jockey-3*. Nascent transcription profiling and total RNA-seq in *Drosophila* embryos show that
85 centromeric and non-centromeric copies of *Jockey-3* are actively transcribed. Using single-molecule RNA FISH
86 combined with immunofluorescence for the centromere protein CENP-C, we show that, during mitosis, *Jockey-3*
87 RNA transcripts localize primarily to centromeres and remain associated with their locus of origin in *cis*. We also
88 show that the presence of CENP-A chromatin is strongly correlated with transcription at both centromeric and
89 non-centromeric full-length *Jockey-3* copies. Furthermore, we find that recent *Jockey-3* transposition events

occur preferentially at CENP-A containing domains across the genome. *De novo* centromere formation *in vivo* using a LacI/lacO tethering system results in the accumulation of lacO transcripts at the *de novo* centromere in mitosis, suggesting that even in the absence of *Jockey-3* or any other centromere-enriched repeats, CENP-A chromatin formation is coupled with transcription *in vivo*. Our work supports a model whereby the *Jockey-3* retroelement targets CENP-A chromatin for its selfish propagation while contributing to CENP-A maintenance through transcription. CENP-A chromatin in itself promotes transcription when artificially assembled. This work provides a framework to understand the persistent association between retroelements and centromeres through evolution.

Results

The transcriptional profile of *Drosophila* centromeres

Transcription of centromeric DNA has been implicated in centromere maintenance in both a sequence-independent manner and through the action of specific transcripts (33, 35-37). In *Drosophila*, only a few known satellite transcripts have been identified (21, 23, 38, 39), but these are either pericentric or not derived from the sequences most highly associated with CENP-A (24). The availability of annotated centromeres for the *Drosophila* laboratory strain iso-1 and the discovery that these centromeres contain retroelements (24) present a unique opportunity to examine transcription across these previously unresolved regions of the genome and explore the correlation with CENP-A occupancy. To identify nascent transcripts, we generated libraries for Precision Nuclear Run-On sequencing (PRO-seq), which detects nascent transcription from RNA polymerase with nucleotide resolution (40) from 0-12h old embryos and 3rd instar larval brains. We also generated RNA-seq libraries for the same type of samples, providing a catalog of stable transcripts. Plotting our PRO-seq data for all genes showed the expected transcriptional profile with a peak at the 5 ’of genes, confirming successful capture of elongating RNA polymerase (**Fig. S1**). Since none of the repeats found at the centromeres are unique to these regions and PRO-seq and RNA-seq generate short-read data, nascent transcripts identified by PRO-seq did not map uniquely to the centromeres using standard mapping methods. To overcome this limitation and determine if any nascent transcripts emanate from centromeric sequences, we adapted a mapping-dependent method recently developed for the human repeats transcriptome (11) to our *Drosophila* datasets. For each dataset, Bowtie 2 default “best match” reports a single alignment for each read providing locus-level transcription profiles (lower bounds); unfiltered Bowtie/Bowtie 2 k-100 mapping reports up to 100 mapped loci for each read, providing over-fitted and locus-level transcriptional profiles (upper bounds); and single copy k-mer filtering, with 21-mers for PRO-seq and 51-mers for RNA-seq data applied to Bowtie k-100, reveals the intermediate bounds of locus-level transcription (**Fig. 1A**). This k-mer filtering requires a given read alignment to overlap with an entire single copy k-mer in the assembly in order to be retained. Together, these different approaches provide a more complete representation of the true transcriptional landscape of centromeres.

We observe nascent transcription at all centromeres, particularly within the islands (**Fig. 1A**). Based on our statistical tests, *Jockey-3* nascent transcripts emerge primarily from full-length *Jockey-3* elements (**Fig. 1B, Fig. S2; Table S1**), 9/23 of which are within the Y centromere, while the rest (14/23) are non-centromeric (**Table 1**). Both centromeric and non-centromeric truncated *Jockey-3* elements are transcribed (**Table S1**), suggesting that the putative promoter at the 5 ’end (Hemmer et al., 2023) is not required for *Jockey-3* transcription. When we compared the number of *Jockey-3* reads mapping to each of the centromeres, classified based on whether they are full-length or truncated, we observed significantly more reads coming from full-length *Jockey-3* insertions within the Y centromere compared to all others (**Fig. 1C**).

Similarly to nascent RNA data, RNA-seq profiles from embryos reveal the presence of transcripts predominantly mapping to the islands, with low levels of satellite transcripts, with the notable exception of

134 AAGAG on the X centromere, which shows more expression in this dataset (**Fig. 1A**). PRO-seq from larval brains
135 (**Fig. S3**), as well as from 0-4h and 4-8h old embryos (data not shown) also showed very similar transcriptional
136 profiles. In contrast, RNA-seq profiles from larval brains showed more transcripts mapping to flanking satellites
137 compared to what we observed in the embryos datasets (**Fig. S3**).

138 To determine more quantitatively which centromere-associated repeats are transcribed, we generated read
139 count plots for each of the repeats found within the centromere contigs. We recreated a density plot of all
140 repetitive elements as in (24) using an updated genome annotation (41) to show how many copies of each
141 repeat are present within each of the centromere contigs (**Fig. 1D**-left plot). We then generated a density heat
142 map for the PRO-seq 0-12h embryos dataset, which displays the total read count for each repeat normalized by
143 the total reads mapping to that contig. This heat map shows that *Jockey-3* is highly expressed at all centromeres
144 relative to other centromeric repeats (**Fig. 1D**-right plot **and Table S2**). Several repeats show background levels
145 of transcription (e.g. *Copia* and *Gypsy-7*), emphasizing that nascent transcription at the centromere occurs
146 primarily at a subset of elements. Collectively, these analyses show that the *Drosophila* centromeres are actively
147 transcribed and that *Jockey-3* in particular contributes significantly to the overall transcription occurring in these
148 regions.

CEN	All	CEN X	CEN Y	CEN 2	CEN 3	CEN 4	CEN (all)	nonCEN
All *Jockey-3*	329	21	147	2	11	21	202	127
FL *Jockey-3*	23 (16)	0 (0)	9 (4)	0 (0)	0 (0)	0 (0)	9 (4)	14 (12)
Truncated *Jockey-3*	306 (26)	21 (3)	138 (5)	2 (0)	11 (0)	21 (1)	193 (9)	113 (17)

149

150 **Table 1: Summary of the location of truncated and full-length (FL) *Jockey-3* insertions with estimated age.**
151 Table showing the distribution of *Jockey-3* copies per centromere, across all centromeres, and across non-
152 centromeric loci. The number of copies with <1% divergence from the *Jockey-3* consensus were deemed 'young'
153 and are indicated in parenthesis. The difference between 'young' and total corresponds to the number of 'old'
154 copies (≥1% divergence).

155

156 ***Jockey-3* transcripts localize to metaphase centromeres**

157 *Jockey-3* is the only element that is transcribed at all five *Drosophila* centromeres (**Fig. 1D**). To examine the
158 subcellular localization of *Jockey-3* transcripts in *D. melanogaster*, we designed strand-specific probes for single-
159 molecule RNA Fluorescence *In Situ* Hybridization (smRNA FISH, henceforth RNA-FISH); one set detects sense
160 transcripts targeting the 5 ʼregion of *Jockey-3*, spanning ORF1, and the other targets the 3 ʼregion, spanning the
161 reverse-transcriptase domain within ORF2 (referred to as ORF1 and ORF2 probes; **Fig. 2A**). We also generated a
162 reverse-complement set of the ORF2 probe to detect antisense transcripts (ORF2 anti). Each of the probe sets is
163 made up of individual oligos that target both centromeric and non-centromeric *Jockey-3* (ORF1 = 44 oligos; ORF2
164 = 45 oligos). Several *Jockey-3* insertions across the genome are targeted by five or more probes, and are thus
165 expected to produce RNA-FISH signal if sufficiently expressed, but centromere contigs are the regions targeted
166 the most because 63% of *Jockey-3* copies are centromeric ((24); **Table 2 and Table S3**). Specifically, the ORF2
167 probe is expected to target primarily the *Jockey-3* copies on centromere X, Y, 3, and 4, while the ORF1 probe is
168 expected to target those from centromere X, Y, 2, and 4.

169 We combined RNA-FISH for *Jockey-3* with immunofluorescence (IF; RNA-FISH/IF) for the centromere protein
170 CENP-C which, unlike CENP-A, is retained on acid-fixed metaphase spreads from larval brain squashes. As a
171 positive control for RNA-FISH, we used a smRNA-FISH probe targeting the *Rox1* non-coding RNA, which coats the

172 X chromosome in males ((42); **Figure S4**). We observed transcripts labeled by the ORF2 probe co-localizing with
173 CENP-C at the X, Y, 3rd, and 4th centromeres (**Fig. 2B, E and S5**), consistent with where these probes sequences
174 map in the assembly (**Table 2 and Table S3**). We also observed co-localization of ORF2 antisense *Jockey-3*
175 transcripts with CENP-C at the same centromeres (**Fig. 2C, E** and **Fig. S5**), indicating the simultaneous presence
176 of both sense and antisense transcripts also shown by our transcript analyses (**Figs. 1 and S3**). Transcripts
177 labeled by the ORF1 probe co-localized with centromeres X, Y, 2, and 4 (**Fig. 2D, E** and **S5**), again consistent with
178 our predictions based on our mapping data (**Table 2** and **Table S3**).

179 The Y centromere is the only centromere containing full-length copies of *Jockey-3* and full-length copies
180 show the highest levels of nascent transcription compared to other centromeres (**Fig. 1C**); thus it is not
181 surprising that the Y displays co-localization between CENP-C and all three probe sets most consistently. In
182 contrast, other chromosomes show more variability in signal detection (**Fig. 2E** and **S5**). In general, the
183 frequency with which we observe co-localization between *Jockey-3* transcripts and CENP-C correlates with the
184 number of probes targeting *Jockey-3* at each particular centromere, with centromere Y being targeted by the
185 most probes overall due to this centromere containing 197/329 total *Jockey-3* copies in the genome ((24)**; Figure**
186 **2E**, **Table 1-2** and **Table S3**). Maximum fluorescence intensity measurements for individual mitotic centromeres
187 followed the same trend, with stronger signal detected on the Y (**Fig. 2F**). All five centromeres– including
188 centromere 2, which contains only two *Jockey-3* fragments next to one another– show colocalization with at
189 least one *Jockey-3* probe set. These findings confirm that truncated as well as full-length centromeric *Jockey-3*
190 copies are active, consistent with our transcriptional profiles (**Figs. 1 and S3**). We also confirmed the localization
191 of *Jockey-3* transcripts at metaphase centromeres in mitotic cells from ovaries and *Drosophila* Schneider cells (S2
192 cells; **Fig. S6 A-B**), confirming that this localization pattern is not unique to larval brain tissues. Furthermore, we
193 performed RNA-FISH/IF on larval brains from *Drosophila simulans*, which diverged from *D. melanogaster* 2.5
194 million years ago (25) and whose centromeres are enriched in *Jockey-3* (24, 27). We observed centromeric foci
195 for *Jockey-3* ORF2 at all mitotic centromeres, indicating that *Jockey-3* expression and transcripts localization is
196 conserved in this species (**Fig. S6C**).

197

RNA-FISH probes mapping	ORF2	ORF2 antisense	ORF1
Cen X	73	73	36
Cen Y	1117	1117	242
Cen 2	4	4	44
Cen 3	70	70	3
Cen 4	130	130	38

198

199 **Table 2. Summary of RNA-FISH probe sequences centromere mapping.** Table showing the total number of
200 *Jockey-3* RNA-FISH probes predicted to bind to each centromeric and non-centromeric contigs. Full mapping
201 across the genome is shown in Table S3.

202

203 To ensure that the signal we observed with our *Jockey-3* probe sets corresponds to RNA and not DNA, we
204 compared staining patterns between RNA and DNA-FISH protocols on brain squashes for the *Jockey-3* ORF2
205 probe and for a DNA-FISH OligoPaint targeting a 100-kb subtelomeric region of chromosome 3L band 61C7 (24).

206 Using our RNA-FISH protocol, we could only detect the signal for *Jockey-3* produced by the ORF2 probe, while
207 with our DNA-FISH protocol (which includes a DNA denaturation step and hybridization in the presence of an
208 RNase cocktail) we only detected signal for the OligoPaint (**Fig. S7**). These experiments confirm that the *Jockey-3*
209 signal shown in **Fig. 2B** corresponds to RNA and not DNA. Treatment with RNase H (which degrades DNA/RNA
210 hybrids) post-hybridization dramatically reduced the signal intensity of *Jockey-3* foci, indicative of degraded DNA
211 probe/RNA hybrids. We also observed a reduction in *Jockey-3* fluorescence when we performed a pre-
212 incubation with an RNase cocktail expected to degrade single stranded RNA prior to RNA-FISH (**Fig. S8**).
213 Together, these controls indicate that the *Jockey-3* transcripts we detect at centromeres with our RNA FISH
214 protocol are *Jockey-3* single stranded transcripts.

215 In addition to localizing to centromeres, *Jockey-3* transcripts also localized to non-centromeric foci on all
216 mitotic chromosomes with the exception of chromosome 4. On average, we observed 1 non-centromeric
217 *Jockey-3* focus per mitotic spread, with a subset of cytological regions displaying foci more frequently than
218 others (*e.g.* middle of XL; **Fig. S9**). Due to gaps in our genome assembly and the limited resolution that can be
219 obtained by microscopy, it was not possible to determine to which *Jockey-3* copies these foci correspond.

220 Centromeric *Jockey-3* foci were also present in interphase cells from larval brains, ovaries, and S2 cells (**Fig.**
221 **S10A-C**). On average, larval brains interphase cells displayed <1 *Jockey-3* focus co-localizing with CENP-C, versus
222 2-3 non-centromeric foci (**Fig. S10D**). Overall, mitotic cells display approximately 3 times more *Jockey-3* foci than
223 interphase ones (**Fig. S10E**). Remarkably, only 15% of interphase cells display 2 or more *Jockey-3* foci co-
224 localizing with CENP-C versus 93% of mitotic cells (**Fig. S10F**). *Drosophila* centromeres are often found clustered
225 together in interphase, which might in part account for this difference. However, PRO-seq and RNA-seq data
226 from larval brains, which reflect primarily the transcriptional state of interphase cells, show low coverage of
227 Jockey-3 transcripts at the centromere islands (**Fig. S3**), consistent with overall lower transcription occurring at
228 the centromere in interphase compared to mitosis. We note that the non-centromeric *Jockey-3* foci observed in
229 interphase could reflect transcripts that remain associated in *cis* or unbound nuclear RNAs.

230 Lastly, to expand on our RNA localization studies, we designed smRNA-FISH probes for another centromeric
231 non-LTR element, *Doc*, which is found within centromere X and 4 and that shows expression (**Fig. 1**). We
232 performed smRNA-FISH/IF on mitotic and interphase cells from larval brains squashes. Unlike *Jockey-3*, *Doc*
233 transcripts were not detectable at the centromeres in metaphase, although the signal was visible in a few
234 interphase cells, where it co-localized with one CENP-C focus (**Fig. S11**). We conclude that not all centromeric
235 retroelements produce transcripts that localize to centromeres in metaphase.

236

237 ***Jockey-3* transcripts co-localize with their cognate sequences in *cis***

238 Studies in human and *Drosophila* cultured cells and in *Xenopus* egg extracts reported that different
239 centromere and pericentromere-derived repeat transcripts can localize to centromeres either in *cis* (*i.e.* at the
240 locus of origin; (9, 21)) or in *trans* (*i.e.* to all centromeres whether or not they contain complementary sequences
241 (12, 23)). Two observations from our data so far point towards *cis* localization of *Jockey-3* transcripts at the
242 centromere. First, the centromeric signal intensity for *Jockey-3* RNA-FISH is positively correlated with the
243 number of probes targeting that centromere (**Fig. 1F** and **Table 1** and **S1**), whereas with *trans* localization, a
244 more uniform signal intensity would be expected, irrespectively of the DNA composition of each centromere.
245 Second, *Drosophila* centromere 2 contains two fragments of *Jockey-3*, one targeted by only 4 out of 44 probes in
246 the ORF2 set and the other targeted by 44 out of 45 probes in the ORF1 set (**Fig. 3A** and **Table 2**) and we observe
247 robust RNA-FISH signal nearly exclusively with the one targeting ORF1 (**Fig. 3B** and **1E**). Conversely, centromere
248 3 *Jockey-3* copies are targeted primarily by ORF2 probes and indeed we observe strong centromeric signals for
249 ORF2 but not ORF1. These observations indicate that RNAs emanating from *Jockey-3* copies colocalize with their
250 cognate DNA sequences in *cis*.

251 To more robustly test if *Jockey-3* transcripts can localize in *trans* to other centromeres, we asked if *Jockey-3*
252 transcripts can be detected on a *de novo* centromere formed on DNA devoid of any centromere-associated
253 repeats. We used a previously developed LacI/lacO system that efficiently forms ectopic centromeres *in vivo* via
254 the tethering of the CENP-A assembly factor CAL1, fused to GFP-LacI, to a 10-kb lacO array inserted at the
255 pericentromere of chromosome 3 (43). We analyzed a total of 89 metaphase spreads from 3 male larval brains
256 by IF/RNA-FISH with anti-CENP-C antibodies and the ORF2 probe and, after imaging, performed sequential DNA-
257 FISH to confirm the location of lacO in the same spreads. We found that, while robust localization of *Jockey-3*
258 ORF2 transcripts at endogenous centromere 3 was clearly visible, *Jockey-3* signal was nearly never observed at
259 the ectopic centromere on lacO (1/90 showed weak signal on one sister; **Fig. 3B-C**). Together, these findings are
260 consistent with *Jockey-3* transcripts remaining associated with the DNA sequences they originated from,
261 similarly to what was reported for centromeric alpha-satellite transcripts in human cells (9).

262

263 **Knockdown of *Jockey-3* RNA does not negatively affect normal centromere function**

264 Knock-downs of alpha-satellite transcripts (44) and of a LINE-1 element associated with a neocentromere
265 (17) lead to a decrease in the levels of CENP-A from the (neo)centromeres these transcripts originate from,
266 suggesting they play a localized role in centromere maintenance or stability. In contrast, in *S. pombe,*
267 centromere-derived transcripts are rapidly degraded by the exosome and are thus unlikely to play such a
268 structural role, but rather appear to be byproducts of centromere transcription (29).

269 To test the possibility that *Jockey-3* transcripts themselves play a role in centromere integrity, we designed a
270 short-hairpin (sh) to target *Jockey-3* RNA for degradation via *in vivo* RNA interference (RNAi). As *Jockey-3* copies
271 are heavily polymorphic in sequence and length, no single sh can target the majority centromeric or genomic
272 copies. We therefore designed a sh targeting the RT domain in ORF2, which is present in ~27% of *Jockey-3*
273 insertions in the genome, targeting as many centromeric and non-centromeric copies as possible (**Fig. 4A**), and
274 generated transgenic flies expressing the sh-*Jockey-3* under a GAL4 UAS promoter.

275 To verify the effectiveness of the knock-down, we induced sh-*Jockey-3* expression under the neural elav-
276 GAL4 driver, isolated total RNA from larval brains, and measured *Jockey-3* expression by RT-qPCR, using primers
277 mapping outside of the sh-*Jockey-3* target. These primers capture 72/80 *Jockey-3* copies targeted by the short
278 hairpin, including 2 centromeric copies on the X, 27 on the Y, 2 on the 3rd, and 3 on 4th chromosome, all of
279 which were confirmed as expressed by PRO-seq. Across three biological replicates, we found that sh-*Jockey-3*
280 expression was reduced by ~44% in sh-*Jockey-3* compared to a sh-mcherry control (**Fig. 4B**). However,
281 measurements of the RNA-FISH signal intensity showed no significant change for *Jockey-3* ORF1 or ORF2 at the Y
282 centromere in metaphase (**Fig. 4C-D**). Similarly, we did not observe a decrease in CENP-C intensity at the Y
283 centromere (**Fig. 4E**), which would have been indicative of a centromere assembly defect, nor did we detect an
284 increase in aneuploidy (N=3 brains, n=25 spreads each, 1.33% aneuploid in sh-*Jockey-3* versus 6.7% in control,
285 p=0.2).

286 RNAi based knockdowns typically affect transcripts post-transcriptionally and their effectiveness in knocking
287 down nuclear RNAs is unclear (discussed in (45)). To determine if the nuclear pool of *Jockey-3* transcripts is
288 reduced upon RNAi, we quantified the total nuclear fluorescence intensity of *Jockey-3* in interphase larval brain
289 cells and found no significant change compared to the control (**Fig. 4F**), suggesting that the decrease in
290 expression observed by RT-qPCR (**Fig. 4B**) reflected changes in the cytoplasmic pool of *Jockey-3*. An alternative
291 explanation is that the *Jockey-3* copies not targeted by the knockdown supply sufficient nuclear RNA signal to
292 obfuscate any reductions caused by the depletion. Nonetheless, consistent with the lack of mitotic defects,
293 expression of the hairpin under the eyeless-GAL4 driver in adult eyes did not cause any disruptions to eye
294 morphology compared to the control (data not shown). We also observed similar progeny viability and fertility in
295 flies expressing sh-*Jockey-3* compared to controls (data not shown). These findings suggest that the cytoplasmic

296 pool of *Jockey-3* RNA is not important for centromere integrity, chromosome segregation, or viability. However,
297 given that this approach does not target all expressed *Jockey-3* copies, we cannot rule out that nascent *Jockey-3*
298 RNA may play a role as a *cis*-acting non-coding RNA at centromeres.

299

300 **CENP-A chromatin profiling reveals a link between *Jockey-3* transcription and CENP-A association**

301 *Jockey-3* is the most enriched repeat in CENP-A chromatin immunoprecipitations (24) and is present at both
302 centromeric and non-centromeric regions of the genome (**Table S1**). However, the non-centromeric occupancy
303 of *Drosophila* CENP-A and its relationship with non-centromeric *Jockey-3* copies has not been explored.
304 Furthermore, we do not know if the presence of CENP-A and the transcriptional activity of *Jockey-3* are
305 correlated. To investigate these questions, we identified significant CENP-A peaks using CUT&Tag (46) from 0-
306 12h embryos, and mapping the resulting sequencing data to the heterochromatin-enriched genome assembly
307 (24). We identified the expected five centromeric CENP-A domains (**Fig. S12**; (24)) along with 333 non-
308 centromeric domains (**Table 3**; **Table S4**). These non-centromeric CENP-A domains were smaller on average and
309 contained lower CENP-A signal intensity than the centromeric ones (**Fig. 5A-B**). Lower CENP-A signal of ectopic
310 compared to centromeric CENP-A was also previously reported for human HeLa cells (47). Next, we examined
311 whether the transcription of *Jockey-3* copies correlated with CENP-A occupancy. There are 202 copies of *Jockey-*
312 *3* that fall within a centromeric CENP-A domain, 26 that fall within a non-centromeric CENP-A domain, and 101
313 that fall in neither (**Table S6**). We found that, while 36% of *Jockey-3* copies within the centromeric CENP-A
314 domains are expressed, this percentage increases to 96% for *Jockey-3* copies at non-centromeric CENP-A
315 regions. Expression of *Jockey-3* copies not CENP-A associated is also high at around 60% (**Fig. 5C; Table S1** and
316 **Table S5**). When we compared all CENP-A associated *Jockey-3* copies with all non-CENP-A associated ones, the
317 difference in the percentage of active *Jockey-3* elements is only 43% versus 62%, respectively (**Fig. 5D; Table S1**
318 and **Table S5**). We conclude that although there is an enrichment of *Jockey-3* elements associated with CENP-A
319 versus not (228/329, or 69%; **Fig. 5E** and **Table S6**), the expression of *Jockey-3* in embryos appears to be
320 independent of its association with CENP-A. However, when we consider only full-length *Jockey-3* copies, which
321 are the most highly expressed copies in the genome (**Fig. 1B**), we see a strong and positive correlation between
322 the association with CENP-A and active transcription (**Fig. 5F; Table S1**), regardless of centromeric location. After
323 breaking down the data by where all full-length *Jockey-3* copies are located (Y centromere, non-centromeric
324 regions, or non-CENP-A associated regions), it is clear that CENP-A association, irrespective of centromeric
325 location, is correlated with higher transcription (**Fig. 5G**). From these analyses, we conclude that full-length
326 *Jockey-3* copies are more highly expressed when coupled with CENP-A chromatin.

327 It is noteworthy to point out that both PRO-seq and CUT&Tag were performed on nuclei from embryos and
328 thus reflect the transcriptional and chromatin profiles of primarily interphase cells. In contrast, the observation
329 that the detection of *Jockey-3* RNA-FISH signal is more frequent at centromeres compared to non-centromeric
330 locations came from metaphase chromosomes (**Fig. S10C**). Even though we cannot directly test this by PRO-seq
331 on mitotic cells, we infer that the proportion of *Jockey-3* transcripts emanating from centromeres versus non-
332 centromeric regions is likely to be higher in mitosis.

333

CEN designation	# CENPA domains	# CENPA domains containing *Jockey-3*
CEN	5 (1/chromosome)	5 (100%)
nonCEN	333	43 (12.91%)

334

335 **Table 3. Summary of the CENP-A domains and associated *Jockey-3* insertions.** Table showing the distribution of
336 CENP-A domains classified as centromeric vs. non-centromeric and the proportion that contains copies of
337 *Jockey-3*.
338
339 **Recent *Jockey-3* insertions are found more frequently within CENP-A chromatin and are more expressed**
340 In *Drosophila*, *Jockey-3* shows weak insertional bias for the centromere (41), but whether such preference
341 relies on specific centromeric sequence features or on the presence of CENP-A is unknown. The observation that
342 *Jockey-3* is also enriched at the centromeres of *D. simulans* (24, 27), even though this species contains widely
343 divergent centromeric repeats (26, 27), suggests that such insertion bias is unlikely to be mediated by DNA
344 sequence preference. If *Jockey-3* preferentially transposes within centromeres through recognition of CENP-A
345 chromatin, we would expect recent insertions to be enriched within both centromeric and non-centromeric
346 CENP-A domains. To test this possibility, we calculated the percentage of young *Jockey-3* insertions (<1%
347 divergence from *Jockey-3* consensus; **Table 1**; (41)) that overlap with CENP-A domains and compared it to the
348 percentage found at non-CENP-A containing regions of the genome. Interestingly, we found that 80% of young
349 copies (34/42) are found in genomic regions that overlap with CENP-A domains, compared to 20% in non-CENP-
350 A containing regions (**Fig. 6A**). Considering that CENP-A domains make up a small percent of the genome, this is
351 a dramatic enrichment. Of these 34 CENP-A-associated *Jockey-3* copies, 13 are centromeric and 21 non-
352 centromeric, consistent with the hypothesis that the retroelement targets CENP-A chromatin for reinsertion
353 irrespective of its centromeric or non-centromeric location. In contrast, old *Jockey-3* insertions (>1% divergence
354 from *Jockey-3* consensus; **Table 1**; (41)) are disproportionately associated with centromeric CENP-A domains
355 rather than non-centromeric ones. One possible explanation for this observation is that non-centromeric CENP-
356 A domains are more dynamic over evolutionary time than centromeres and thus, as retroelement insertions in
357 those regions age, they end up no longer being CENP-A associated.

358 The presence of CENP-A on full-length *Jockey-3* copies is associated with higher transcription (**Fig. 5G**). We
359 hypothesized that *Jockey-3* preferentially inserts within CENP-A chromatin to increase its chance of being
360 expressed. If this were the case, we would expect recent insertions to be more highly expressed if associated
361 with CENP-A than not. We counted the number of PRO-seq reads mapping to CENP-A associated and non-CENP-
362 A associated *Jockey-3* insertions classified as young or old (**Table 1**) and found that newer insertions within
363 CENP-A chromatin are significantly more expressed than those at non-CENP-A domains (**Fig. 6B**). Older
364 insertions are overall less expressed than young ones. Interestingly, young CENP-A associated copies, which are
365 primarily non-centromeric (**Fig. 6A**) are also more expressed than their older counterparts, which are primarily
366 centromeric. However, the centromeric *Jockey-3* copies are also largely truncated, which we showed are
367 generally less transcribed (**Fig. 1B**). Collectively, these observations suggest a model where *Jockey-3* has evolved
368 the ability to target CENP-A for insertion to promote its expression. Due to its role at centromeres and its
369 requirement to be transcriptionally permissive, CENP-A chromatin may be spared by genome-defense
370 mechanisms that target transposons for silencing, providing a protective environment for *Jockey-3*.
371
372 ***lacO* transcription is coupled with *de novo* centromere formation**
373 All our data so far points to a correlation between CENP-A chromatin and *Jockey-3* expression. Therefore, we
374 next investigated if DNA associated with *de novo* centromeres, which lack *Jockey-3* or other centromere repeats,
375 is also transcribed. In *Drosophila* S2 cells and flies *de novo* centromeres are efficiently formed when the CENP-A
376 chaperone CAL1 is fused to GFP-LacI and tethered to a lacO array inserted within the genome (43, 48). Upon its
377 tethering to the lacO array in S2 cells, CAL1, alongside the elongation factor FACT and RNA polymerase II, initiate
378 transcription of non-endogenous sequences belonging to the inserted lacO array (16).

379 To determine if the DNA associated with a *de novo* centromere becomes transcribed *in vivo*, we used an
380 oligo lacO probe to detect lacO-derived transcripts by RNA-FISH in larval progeny expressing CAL1-GFP-LacI or a

381 GFP-LacI control under the neural elav-GAL4 promoter and heterozygote for a pericentric 10-kb lacO array
382 inserted at 3L (3^{peri} at cytoband 80C4; (43)). Consistent with previous studies, expression of CAL1-GFP-LacI
383 results in ectopic centromere formation at the 3^{peri} lacO array in more than 80% of spreads (43). We performed
384 sequential IF-RNA/DNA-FISH on mitotic spreads from larval brains in elav-GAL4, CAL1-GFP-LacI and GFP-
385 LacI/lacO expressing progeny. IF for CENP-C was used to identify active centromeres and lacO RNA-FISH allowed
386 us to establish if transcripts are visible at ectopic centromeres. After imaging metaphase spreads, we processed
387 the slides for DNA-FISH with the same lacO probe to identify the position of the lacO array. We also included a
388 probe for the peri/centromeric satellite *dodeca* to identify the endogenous centromere 3s, and re-imaged the
389 same mitotic spreads. We found that both GFP-LacI control spreads and CAL1-GFP-LacI/3^{peri} spreads display lacO
390 RNA-FISH signal, but the latter show significantly higher frequency compared (**Fig. 7A-B**). In interphase, we
391 found that there is no significant difference in lacO transcription frequency between CAL1-GFP-LacI/3^{peri} and
392 GFP-LacI/3^{peri} in interphase cells (**Fig. 7C**), suggesting that the higher transcription frequency observed in CAL1-
393 GFP-LacI/3^{peri} is specific to metaphase. To determine if lacO expression levels are different between GFP-LacI
394 and CAL1-GFP-LacI/3^{peri} mitotic spreads, we measured lacO RNA fluorescence intensity for both genotypes and
395 found that CAL1-GFP-LacI/3^{peri} displays higher lacO RNA signal intensity than the GFP-LacI/3^{peri} control (**Fig. 7D**).
396 Collectively, these experiments demonstrate that although lacO is transcribed in the absence of an ectopic
397 centromere, transcription is observed at a higher frequency and at higher levels when an ectopic centromere is
398 present, suggesting that the formation of a *de novo* centromere stimulates local transcription. These results are
399 consistent with previous reports in human neocentromeres (17, 19, 49) and *de novo* centromeres in S2 cells (16)
400 showing increased transcription upon CENP-A chromatin formation at non-centromeric sites. They also further
401 underscore the correlation between CENP-A deposition in mitosis and an increase in transcription.

402

403 ## Discussion

404 In this study, we examined the transcriptional landscape of *Drosophila* centromeres and identified the
405 centromere-enriched retroelement *Jockey-3* as a key transcribed component across these regions. We found
406 that *Jockey-3*, produces transcripts that accumulate at all mitotic centromeres, a localization that is conserved in
407 *D. simulans*. In metaphase, *Jockey-3* transcripts remain associated with their cognate DNA sequences and do not
408 diffuse to other native nor *de novo* centromeres. Metaphase is the cell cycle stage that coincides or precedes
409 (depending on cell types and species) metazoan CENP-A deposition (50-56). A boost in transcription before or
410 around the time of CENP-A deposition could prime chromatin by removing place-holder histone H3.3 (57) to
411 allow the assembly of CENP-A nucleosomes. Consistent with this model, active RNA polymerase II (RNAPII)
412 and/or transcriptional activity has been reported at metaphase centromeres in both *Drosophila* (21, 23) and
413 human cell lines (9, 11, 30). In human cells, RNAPII is lost from chromosome arms upon cohesin degradation in
414 prophase, yet persists at centromeres in metaphase where cohesin remains enriched until anaphase (58).

415 To inform on whether the act of transcription is important for CENP-A maintenance, previous studies used
416 transient treatments with RNA polymerase inhibitors. In *Drosophila* S2 cells, transcriptional blockage
417 destabilized the chromatin association of new CENP-A at centromeres (21). Somewhat surprisingly, RNA
418 polymerase inhibitors injected into early *Drosophila* embryos did not result in a decrease in centromeric GFP-
419 CENP-A signal intensity, which would be expected if transcription was required for *de novo* GFP-CENP-A
420 deposition (59). However, it is unclear if CENP-A deposition during the rapid divisions occurring at this
421 developmental stage involves eviction of place-holder histone H3.3.

422 There are 329 copies of *Jockey-3* in the *Drosophila* genome, 202 of which (61%) are found within the five
423 centromere contigs (24, 41). Analyses of nascent transcripts reveal that the *Jockey-3* copies present within the
424 centromeres are not expressed at higher levels than those found elsewhere in the genome –in fact, at least in
425 interphase, *Jockey-3* elements within the centromeres are overall expressed at lower levels– suggesting that the

426 expression of *Jockey-3* elements is not linked to their centromeric location. These results are consistent with
427 studies in human RPE cells that showed that alpha-satellite transcripts are produced from both centromeric
428 arrays and from arrays outside of the active human centromere region (9). It is possible that the accumulation of
429 *Jockey-3* and other expressed repeats at the centromere might underscore selection for transcriptionally active
430 elements in these regions to facilitate CENP-A chromatin maintenance.

431 Full-length *Jockey-3* copies contribute the most to overall *Jockey-3* transcription, and the majority of these
432 full-length copies are found at non-centromeric loci (14/23). Interestingly, we find that the expression of these
433 full-length *Jockey-3* copies is strongly positively correlated with CENP-A occupancy. Our PRO-seq profiles reflect
434 nascent transcription in interphase, and at this cell cycle stage the co-localization of *Jockey-3* RNA signal with
435 centromeres is detected less frequently and at fewer centromeres than in metaphase. In contrast, RNA-FISH on
436 metaphase chromosomes reveals bright *Jockey-3* RNA foci primarily at centromeres. The observation that
437 transcripts from the expressed centromere-associated retroelement *Doc* do not localize to metaphase
438 centromeres, unlike those from *Jockey-3*, suggests that *Jockey-3* may have a unique ability for enhanced
439 transcription during this stage. The RNA signal is especially strong on the mitotic Y centromere, which contains
440 an abundance of expressed *Jockey-3* copies. It is interesting to note that the Y centromere also displays stronger
441 CENP-A signal in spermatocytes and early embryos (60), consistent with the possibility that high levels of CENP-A
442 may be linked to abundant *Jockey-3* expression and/or the retention of its RNA products.

443 While centromere-associated *Jockey-3* transcripts are visible with high frequency in metaphase, non-
444 centromeric foci are more rare and certainly fewer than the 127 known non-centromeric *Jockey-3* insertions or
445 the 14 full-length non-centromeric copies. In interphase too, the number of non-centromeric foci is much
446 smaller than the number of non-centromeric *Jockey-3* copies. It is possible that different insertions alternate
447 between active and inactive states. Alternatively, only a subset of full-length *Jockey-3* copies produce sufficient
448 nascent transcripts to be detectable by RNA-FISH.

449 Our finding that *de novo* centromeres are coupled with transcriptional activation of the underlying DNA
450 specifically in metaphase reinforces the model that CENP-A deposition and transcription go hand in hand. Our
451 experiments do not distinguish between transcriptional activation of lacO being caused by CAL1 tethering, given
452 that CAL1 is known to interact with RNAPII and FACT (16), or being linked to active CENP-A deposition. However,
453 the latter possibility would be consistent with recent studies in human neocentromeres showing that
454 neocentromere formation is associated with transcriptional activation and increased chromatin accessibility (18,
455 19).

456 The *Jockey-3* retroelement is enriched at the centromere compared to the rest of the genome in *D.*
457 *melanogaster* and *D. simulans* (24, 27). How this retroelement has accumulated at centromeres over time
458 remains a matter of speculation, but population studies show that low frequency polymorphic insertions,
459 indicative of recent transpositional events, show a weak bias towards centromeres (61). Using divergence from
460 the consensus to estimate the age of the element (61), we found that much of the most recent transposition
461 events have occurred within regions containing CENP-A. Given that the majority of non-centromeric CENP-A
462 domains do not overlap with a *Jockey-3* element, we speculate that it is *Jockey-3* that follows CENP-A rather
463 than the other way around. Regardless of whether CENP-A or *Jockey-3* come first, recent *Jockey-3* copies are
464 more transcribed than old ones, suggesting that a new insertion has the potential to affect CENP-A chromatin,
465 which could result in its stabilization or its disruption.

466 The centromeres of three species within the *Drosophila simulans* clade–*D. simulans*, *D. mauritiana*, and *D.*
467 *sechellia*–and *D. melanogaster*, display a remarkable turnover in sequence composition, suggesting the
468 existence of a genetic conflict between satellites and retroelements (27). To ensure their own propagation
469 through generations, these selfish genetic elements appear to compete for dominance at the centromere, a
470 region with low recombination that can tolerate variation in sequence composition without loss of functionality.

Since *Jockey-3* is targeted by piRNA-mediated silencing in the germline (61), its preferential insertion at centromeres could provide an advantage for its continuous propagation since centromeres are typically not associated with heterochromatic marks (3, 27, 61, 62). Given the rapid evolution of centromere repeats and the lack of uniformity even within the five centromeres of *D. melanogaster*, targeting CENP-A chromatin preferentially represents an efficient way for *Jockey-3* to end up at centromeres. In turn, *Jockey-3* could benefit the host by promoting local transcription, which could facilitate chromatin remodeling during CENP-A deposition. Changes in expression for LINE1 modulate global chromatin accessibility during early mouse embryonic development, independently of both the LINE1 RNA or its protein products (63). Similarly, *Jockey-3* expression could promote local chromatin accessibility at centromeres. Future work will need to explore if the retention, the metaphase transcription of *Jockey-3*, or neither, are required for the integrity and maintenance of centromeric chromatin.

Global analyses of the chromatin-associated non-coding transcriptome in human embryonic stem cells showed that most RNA-DNA interactions are proximity based, with virtually none occurring in *trans*. Furthermore, TE-derived RNAs are frequently found associated with chromatin (64). Our results showing *cis* localization of *Jockey-3* are consistent with these findings. Even though we did not observe RNA-FISH signal in metaphase for the centromere-associated *Doc* retroelement, it is possible that additional centromere-derived RNAs contribute to the overall regulatory output of RNA-chromatin interactions at the centromere, similar to that proposed for genes (64).

Why *Jockey-3* RNAs are retained at centromeres remains unclear. RNA localization evidence does not differentiate between RNAs that are tethered to the centromere through the active transcriptional machinery from those complexed with centromeric proteins. These transcripts may simply be an incidental byproduct of the element's transcription with no further regulatory role (45) or, like alpha-satellite RNAs, they could interact with centromeric proteins contributing to centromere integrity (9). Alternatively, transcript retention could serve as a mechanism for regulating *Jockey-3* transposition: it may function as an integral part of this retroelement's mechanism of transposition or, conversely, as a defense strategy employed by genomes to prevent the transposon's re-insertion in gene-encoding genomic regions.

Jockey-3 transcripts form distinct, bright foci at metaphase centromeres, bearing similarity to RNA-rich nuclear condensates such as histone locus and Cajal bodies, or nucleoli (65). RNA has the ability to initiate condensate formation, supporting the nucleation of additional RNAs and proteins (66). In *S. pombe*, clustering of the centromeres by the Spindle Pole Body facilitates CENP-A assembly through this structure's ability to attract high concentrations of CENP-A and its assembly factor (20). It is possible that high concentrations of *Jockey-3* transcripts produced in metaphase may aid in the maintenance of centromeres by attracting elevated levels of *Drosophila* CENP-A and its assembly factor CAL1 (48). This mechanism could depend more on the origin of the RNA (specifically, its derivation from centromeres) than its unique sequence.

Acknowledgements

We would like to thank Bo Reese from the UConn the Center for Genome Innovation in the Institute for Systems Genomics for assistance with sequencing and Vijender Singh (Computational Biology Core, Institute for Systems Genomics) and the UConn High Performance Computing for computational support. We are grateful to Jason Palladino and members of the Mellone lab for discussion and suggestions. This work was funded by NIH R35GM131868 to BGM. Additional support: NIH R01GM123312 to RJO, NSF MCB1844693 to AML, and NIH R35GM128857 to LC.

513

514 **Author contribution statement**

515 Conceptualization: BM. Project administration: BM. Investigation: BS, RS, AA, OL, CC, LL. Formal analyses: BS,
516 RS, AA, SJH, RD, BM. Visualization: BM, BS, RS, AA, SJH. Resources: BM, LC, AML. Methodology: All authors.
517 Software: AA, SJH, RD. Validation: BM, BS, RS, AA, SJH. Supervision: BM, AML, LC, RJO. Writing- Original draft:
518 BM, RS, SJH, BS, AA. Writing- Review and Editing: BM, RS, AA, SJH, BS, RJO. Funding Acquisition: BM, RJO, AML,
519 LC.

520 # Methods

521 ***Drosophila* stocks and handling**

522 Flies were reared on standard cornmeal, molasses, and yeast food (https://bdsc.indiana.edu) at 25°C, except
523 for crosses for RNAi and sh-mediated knockdowns, which were carried out at 29°C. Experiments were
524 performed in the following *D. melanogaster* stocks: laboratory stock iso-1 (Bloomington Drosophila Stock Center
525 stock no. 2057: y1; Gr22b^{iso-1} Gr22d^{iso-1} cn^{1} CG33964^{iso-1} bw^{1} sp^{1}; MstProx^{iso-1} GstD5^{iso-1} Rh6^{1}); laboratory stock
526 OreR (from A. Spradling lab); lacO (3^{peri}, cytoband 80C4); UAS-CAL1-GFP-LacI and UAS-GFP-LacI maintained as
527 heterozygous lines with the T(2;3)TSTL double balancer (43); sh-mCherry (Bloomington Drosophila Stock Center
528 stock no. 35785) and sh-*Jockey-3*; gCID-EGFP-CENP-A/CID (P{gcid.EGFP.cid}III.2; (67) . The GAL4 driver used was
529 elav-GAL4 balanced with T(2;3)TSTL translocation balancer. The *D. simulans* stock used is w501 (gift of Andy
530 Clark).

531 For all knockdowns, elav-GAL4 balanced with T(2;3)TSTL males were crossed with sh virgin females at 29°C.
532 Non-tubby larvae, which carried both elav-GAL4 and the sh, were selected for dissections.

533 The sh-*Jockey-3* line was generated by PhiC31-mediated integration of pVALIUM20-sh-*Jockey3* at the attP2
534 landing site after injection by a commercial service (Best Gene). The *Jockey-3* hairpin was designed against the
535 reverse-transcriptase region of *Jockey-3* using the DSIR website (http://biodev.extra.cea.fr/DSIR/DSIR.html),
536 picking the one with the highest score. The sequences targeting *Jockey-3* were: 5'-ACGCTGGAACATCATGATCAA
537 (Passenger strand) and 5'-TTGATCATGATGTTCCAGCGT (Guide strand). The oligos ordered included the
538 passenger and guide strands flanked by standard flanking sequences. The resulting oligos were: 5'-
539 ctagcagtACGCTGGAACATCATGATCAAtagttatattcaagcataTTGATCATGATGTTCCAGCGTgcg (Top strand) and 5'-
540 aattcgcACGCTGGAACATCATGATCAAtatgcttgaatataactaACGCTGGAACATCATGATCAAactg (Bottom Strand). These
541 top and bottom strands were annealed together creating overhangs and ligated into pVALIUM linearized with
542 NheI and EcoRI.

543

544 **Cell culture**

545 *Drosophila* Schneider (S2) cells were grown in Schneider's media containing 10% FCS and anti-biotic/anti-
546 mycotic mix at 25°C. Cells were passaged twice a week by diluting a cell resuspension to a million cells/ml.

547

548 **Stellaris probe design**

549 Custom probes were designed using the Stellaris FISH probe designer. Probes were designed against the
550 *Jockey-3* consensus sequence using ORF1 and ORF2 as targets. See Table of reagents for probes sequences.

551

552 **RNA extraction from brains and RT-qPCR**

553 20-30 male larval brains were dissected in ice cold PBS DEPC and preserved in 150µl RNA later at -20°C. PBS
554 DEPC was added to the brain suspension and spun to pellet the brains. The PBS/RNA later was removed and the
555 brains were lysed in 300µl of TRIzol using a motorized pestle. RNA was extracted with Zymo Direct-zol RNA
556 MiniPrep Kit (Cat#: 11-330) according to manufacturer's instructions, except the in-column DNase I treatment
557 was repeated twice. Samples were then treated with Turbo DNAse 2 to 3 times and then purified with the RNA
558 Clean and Concentrator-5 Kit (Zymo Research Cat#: 11-325) according to the manufacturer's instructions. cDNA
559 was prepared with iScript Reverse Transcription Supermix following the manufacturer's instructions. PCR was
560 used to check cDNA quality and no DNA contamination in the no reverse transcriptase samples. qPCR was

561 performed with iTaq Universal SYBR Green Supermix in 96 well plates, and ran on a BioRad qPCR thermocycler.
562 Relative quantity was calculated with the Pfaffl method (68).

563 The PCR cycle was as follows: 95 °C 3 min for initial denaturation, then followed by 40 qPCR cycles. Each cycle
564 has denaturation at 95 °C for 10s, annealing at 55°C for 20s and extension at 72°C for 20s.

565

566 **Primer design for targeting *Jockey-3***

567 We designed primers targeting the reverse-transcriptase domain within ORF2 from the *Jockey-3* consensus
568 sequence using the Primer Design tool in Geneious Prime, avoiding the sequence targeted by the sh-*Jockey-3*
569 itself. To determine which genomic copies are likely captured by these primers, we mapped the primers to the
570 list *Jockey-3* insertions targeted by sh-*Jockey-3*, using the Map to Reference tool in Geneious Prime, allowing a
571 maximum of 3 mismatches.

572

573 **Metaphase spread preparations from larval brains**

574 All solutions were made up in DEPC milliQ water. Third instar larval brains were dissected (2-3 brains/slide) in
575 PBS and all attached tissue and mouth parts were removed with forceps. Brains were immersed in 0.5% sodium
576 citrate solution for 8 min in a spot well dish then moved to a 6µl drop of 45% acetic acid, 2% Formaldehyde on a
577 siliconized (Rain X-treated) coverslip for 6 min. A poly-lysine coated glass slide was inverted and placed on the
578 brains to make a sandwich. After flipping the slide and gently removing excess fixative between bibulous paper,
579 the brains were squashed with the thumb by firmly pressing down. Slides were then immersed in liquid nitrogen
580 and the coverslip was flipped off using a razor blade. Slides were then transferred to PBS for 5 min to rehydrate
581 before proceeding with RNA-FISH/IF or IF/RNA-FISH. Monolayers brain preparation were performed using the
582 same procedure except that acetic acid was omitted from the fixative.

583

584 **Mitotic spread preparations from S2 cells**

585 $3x10^5$ Schneider (S2) cells were collected in a tube for each slide and media was added to reach a volume of
586 475µl. The cells were treated for 1 hr with 0.5µg/ml colcemid (Sigma Aldrich) to induce mitotic arrest. Cells were
587 then spun at 600g for 5 min in a centrifuge and resuspended in 250µl of 0.5% sodium citrate (DEPC treated) for 8
588 min. The cell suspension was loaded into a cytofunnel and spun for 5 min at 1200 rpm onto a poly-lysine coated
589 slide using a cytocentrifuge (Shandon Cytospin 4, Thermo Fisher Scientific). The slides were immediately
590 transferred to a coplin jar containing 100 ml of fixative (45% acetic acid and 2% formaldehyde in DEPC water) for
591 6 min. Slides were then washed 3 times with PBST (0.1% Triton) for 5 min while rocking at room temperature.
592 Slides were stored in 70% ethanol at 4°C until IF/RNA-FISH.

593

594 **Mitotic spread preparations from ovaries**

595 Ovary mitotic preparations were conducted as in (69). Mated adult females were anesthetized with CO_2,
596 then moved to a fresh 50 µL drop of PBS. Whole ovaries were dissected out and the carcass discarded. Using a
597 needle, the tips of the ovaries were separated from later stages and immersed in 0.5% sodium citrate for 5 min,
598 followed by fixation for 4 mins in 2 mL of fixative solution (45% acetic acid, 2.5% formaldehyde). Fixed tissues
599 were moved to a 3 µL drop of 45% acetic acid on a siliconized coverslip (Rain X) and gently teased apart with a
600 needle. A poly-L lysine coated glass slide was inverted onto the coverslip and pressed gently to spread the liquid
601 to the edges of the coverslip. The slide and coverslip were squashed for 2 minutes using a hand clamp (Pony
602 Jorgensen 32225), then immersed into liquid nitrogen for at least 5 minutes. Coverslips were immediately

603 removed using a razor blade. The slide was then dehydrated by placing it in ice cold 70% ethanol for 2 hr at 4°C,
604 and processed for RNA-FISH/IF.

605

606 **RNA-FISH/IF**

607 Slides were immersed in PBST (0.1% Triton) and rocked for 10 min 3 times. Slides were transferred to 70%
608 ethanol at 4°C overnight. Slides were rehydrated in PBST for 5 min and washed in wash buffer (2x SSC and 10%
609 formamide) for 5 min while rocking. Without drying the brains, 50µl probe mix containing 45µl of Hybridization
610 buffer (Stellaris), 5µl Formamide (10% formamide final) with 0.5µl of 12.5µM Stellaris smRNA FISH probes
611 (0.125µM final concentration for Stellaris *Jockey-3* ORF1, ORF2, ORF2 antisense, *Doc*, *Rox1*). Brains were covered
612 with a HybriSlip coverslip, sealed with rubber cement to prevent evaporation, and incubated at 37°C overnight
613 in a humid chamber. Slides were then rinsed twice with wash buffer, washed twice in washing buffer for 30 min,
614 and three times with 2X SSC for 10 min while gently shaking at RT. Slides were then post-fixed for 10 min in the
615 dark in 100µl of 3.7% formaldehyde in PBS DEPC.

616 After 3 additional 5 min washes in PBST, the slides were then transferred to a coplin jar containing blocking
617 buffer (1% BSA in PBST; PBS, 0.1% Triton-X) for 30 min while rocking. 50µl of primary antibodies (anti-CENP-C
618 guinea pig polyclonal antibodies, 1:500) diluted in blocking buffer were applied to the slides, covered with
619 parafilm and stored in a dark chamber at 4°C overnight. The following day, slides were washed 4 times with
620 PBST for 5 min while rocking. Secondary antibodies (goat anti-guinea pig A488, 1:500) diluted in blocking buffer
621 were applied to the brains, covered with a square of parafilm and incubated at room temperature for 1 hr.
622 Slides were then washed 4 times in PBST for 5 min while rotating and again quickly in PBS for 3 min. Slides were
623 mounted using SlowFade Gold containing 1µl/ml DAPI and a 22x22mm coverslip sealed with nail polish. The
624 slides were stored in a dark environment to dry for 10 min before imaging.

625

626 **IF/RNA-FISH**

627 Slides containing squashed larval brains were washed 3 times with PBST for 5 min on a rotator and
628 transferred to 70% ethanol diluted at 4°C for 1 hr. Slides were then rehydrated for 5 min in PBST and processed
629 for IF as described in the RNA-FISH/IF method above. After washing off the secondary antibodies, the slides
630 were then processed for RNA-FISH without post-fixing, using Stellaris probes for *Jockey-3* and a lacO LNA probe
631 Slides were mounted as described for RNA-FISH/IF.

632

633 **Sequential IF/RNA-FISH/DNA-FISH to detect lacO RNA at *de novo* centromeres**

634 IF/RNA-FISH samples (anti-CENP-C guinea pig 1:500; lacO LNA, *Jockey-3* ORF2) were imaged and the list of
635 points visited was saved. Coverslips were removed with a razor blade and the slides were washed in PBS for 10
636 min at room temperature while rocking. Slides were then washed three times with 4X SSC for 3 min, once with
637 2X SSCT for 5 min, and once with 50% formamide 2X SSC for 5 min at room temperature while rocking. 50 µl
638 probe mix containing 13.5 µl 4X hybrid mix (8X SSC, 0.4% Tween20, 40% dextran sulfate, 34 µl formamide, 2µl
639 RNase cocktail, 0.5 µl lacO LNA probe (100µM stock), 0.5 µl *dodeca* LNA probe (100µM stock) were added to the
640 slide, covered with a hybrislip and sealed with rubber cement. Slides were incubated at 95°C for 5 min in a slide
641 thermal cycler (Epperndorf) then transferred to a humid chamber and incubated at 37°C overnight in the dark.
642 After incubation, the hybrislip and rubber cement were removed. Slides were then washed once at 37°C with
643 0.1X SSC for 10 min and twice at room temperature with 0.1X SSC for 10 min while rocking. Slowfade Gold
644 containing DAPI was applied to the brains, covered with 22X40 mm or 22X22 mm coverslips, and sealed with nail
645 polish. Imaging was performed by re-visiting the same point list.

646

647 **RNase treatments and quantification**

648 For the RNase H treatments, male 3rd instar larval brain monolayers from a line expressing CENP-A/CID-EGFP
649 under the control of the CENP-A/CID regulatory sequences (67) were processed for RNA-FISH using the *Jockey-3*
650 ORF2 probe. Two slides were prepared. The following day, samples were imaged and point locations were
651 recorded. Following imaging of these two pre-treatment slides, the coverslips were removed and the slides were
652 briefly rinsed in PBS. RNase H treatment was performed with 10U of RNase H (cleaves the RNA when coupled
653 with DNA; NEB) incubated for 2hr at 37°C in a dark humid chamber on one the slides, while the control slide was
654 treated in the same way omitting the RNase H but including the buffer diluted in water. Slides were then
655 washed once with PBS and mounted as described. The slides were then reimaged using the same settings as
656 before, with the same points revisited. Quantification of the samples were done by counting the number foci of
657 eCENP-A/CID-GFP and *Jockey-3* ORF1 probes within cells between the pretreatment and post-treatment. Values
658 were plotted using Prism as a scatter plot. Statistical analysis was conducted using the t-test (unpaired).

659 For the RNase cocktail treatment, we generated male 3rd instar larval brain monolayers from eCID-GFP lines.
660 Prior to RNA-FISH probe hybridization, 4U of RNase cocktail (RNase A and RNase T1, both targeting single-
661 stranded RNA; Thermo Fisher) diluted in PBS was added to one slide (treated), while the other slide (untreated)
662 only contained PBS. Samples were incubated at 37°C for 30 min. Samples were then washed for 5 min in PBS and
663 hybridized with the *Jockey-3* ORF2 probe and Rox1 probes RNA-FISH. The following day the samples were
664 imaged and point locations were recorded. Quantification of the samples was done by counting the number
665 eCID-GFP and *Jockey-3* ORF2 foci within cells (N=100 cells) for both samples. Values were plotted as a scatter
666 plot using Prism. Statistical analysis was conducted using the t-test (unpaired).

667

668 Our attempts to degrade the *Jockey-3* RNA-FISH signal from metaphase spreads with RNase H and RNase
669 cocktail treatments were not successful, despite seeing *Rox1* signal become very weak or disappear. We
670 hypothesize that the centromere/kinetochore protects *Jockey-3* RNA from degradation. We also performed
671 these treatments after reversing the crosslinking at 80°C for 8 min as described in (21). However, heat treatment
672 eliminated all *Jockey-3* RNA-FISH signal even in the absence of any RNase, precluding us from drawing any
673 conclusions from these experiments.
674

675 **Imaging**

676 All images were acquired at 25°C using an Inverted Deltavision ULTRA (Leica) equipped with a sCMOS
677 pco.edge detector camera and with either a 100x/1.40 NA or 60x/1.42 NA oil objective using 0.2µm z-stacks.
678 Mitotic spreads were imaged using the 100x objective. Tissue monolayers were imaged using either the
679 60x/1.42 NA or 100x/1.40 NA oil objectives. Image acquisition was performed using DeltaVision Ultra Image
680 Acquisition software and image processing was performed using softWoRx software (Applied Precision). Images
681 were deconvolved for 5 cycles using the conservative setting. All Stellaris probes for RNA-FISH were excited for
682 0.5s at 100% transmission for each z-slice image. Following deconvolution, images were quick-projected as
683 maximum intensity projections using in-focus z-slices, a uniform scale was applied before saving images as
684 Photoshop files. Images were minimally adjusted using Photoshop (Adobe) and assembled into figures in
685 Illustrator (Adobe).

686

687 **Colocalization quantification for *Jockey-3* at centromeres**

688 Metaphases were inspected in the CENP-C channel to identify centromeres and the presence of *Jockey-3*
689 signal was determined by eye and recorded as colocalizing if present in at least one sister.

690

691 **Colocalization quantification for *Jockey-3* at *de novo* lacO centromeres**

692 The presence of dicentrics causes chromosome breaks and rearrangements, making the identification of
693 chromosomes difficult. Therefore, we selected metaphases with intact chromosome 3's (identified with *dodeca*
694 DNA-FISH) and with CENP-C signal at the 3peri location (identified with lacO DNA-FISH) for quantification. For
695 the cis/trans *Jockey-3* ORF2 RNA quantification, the presence of *Jockey-3* RNA signal in the corresponding RNA-
696 FISH images was determined by eye and recorded as present or absent. To determine if lacO transcripts were
697 present, lacO RNA signal was determined by eye and recorded as present or absent. We selected metaphases
698 with intact chromosome 3's (identified with *dodeca* DNA-FISH) and with lacO at the 3peri location (identified
699 with lacO DNA-FISH) for quantification.

700

701 **Fluorescence intensity quantifications**

702 To measure *Jockey-3* signal at the centromeres of metaphase chromosomes, non-deconvolved in-focus z
703 slices were quick-projected using the max intensity setting in SoftWorx. Polygons were drawn around the
704 centromere of each chromosome using the edit polygons tool in the CENP-C channel then propagated to the
705 *Jockey-3* channel to capture *Jockey-3* RNA max intensity fluorescence at the centromere. Similar polygons were
706 used to capture background fluorescence for downstream calculations. Signal for sister centromeres were
707 averaged and the average max intensity of the background fluorescence for that channel was subtracted. The
708 measured max intensities for CENP-C and *Jockey-3* were plotted using Prism and compared.

709 For the quantification of metaphase spreads from sh-*Jockey-3* knockdowns, non-deconvolved 100x images
710 were quick-projected in Softworks using the average intensity setting. Images were exported as TIFF and
711 quantified with FIJI. In FIJI, a 400x400 pixel area including CENP-C, *Jockey-3* ORF1, and *Jockey-3* ORF2 foci on
712 centromere Y was drawn to measure total intensities. Background intensities were set as lowest intensities in
713 the square. Final fluorescence intensities in arbitrary units were calculated by subtracting background intensities
714 from total intensities.

715 For the quantification of interphase spreads from sh-*Jockey-3* knockdowns, images were quick-projected in
716 Softworks using the max intensity setting. Images were exported as TIFF and quantified with FIJI. In FIJI, entire
717 nuclei were circled to measure raw max intensities of CENP-C, *Jockey-3* ORF1, and *Jockey-3* ORF2. Circles were
718 then moved to the background area to measure background intensities. Final fluorescence intensities in
719 arbitrary units were determined by subtracting background intensities from max intensities.

720 For the quantification of metaphase spreads from CAL1-GFP-LacI, *lacO* 3^{peri} and GFP-LacI, *lacO* 3^{peri} , non-
721 deconvolved 100x images were quick-projected in Softworks using the maximum intensity setting. Images were
722 exported as TIFF and quantified with FIJI. In FIJI, a 400x400 pixel area including *lacO* foci on chromosome 3 was
723 drawn to measure the total intensity. The background intensity was set as the average of 8 surrounding 400x400
724 pixel areas. The final fluorescence intensity in arbitrary units was calculated by subtracting the background
725 intensity from the total intensity.

726

727 **Mapping *Jockey-3* RNA-FISH probes to centromeres**

728 To determine how many probes are predicted to bind to each centromere, we mapped probes to the
729 centromeric contigs extracted from the heterochromatin-enriched genome assembly from (24) using the map to
730 reference tool in Geneious, using all default settings and allowing all best matches.

731

732 **Embryo collection, RNA extraction, and nuclei isolation for PRO-seq**

733 Embryos were collected from 2-3 days old iso-1 flies at 25°C. Adult flies were kept in multiple cages on grape
734 juice agar plates containing a small amount of fresh yeast paste. Collection plates from the first 1h were
735 discarded and flies were allowed to lay embryos on grape juice agar plates for 12 hrs overnight. Embryos were
736 rinsed thoroughly with water and egg wash (0.7% NaCl made in DEPC treated water plus 0.05% Triton-X 100) in a
737 mesh basket. Embryos were then dechorionated with 50% bleach for 1 minute, rinsed thoroughly with tap water
738 in a mesh basket, flash-frozen in liquid nitrogen, and stored at -80°C.

739 For RNA-seq, frozen embryos were resuspended in 300µl of TRI Reagent (Sigma Aldrich T9424) and
740 homogenized using a motorized pestle. After centrifugation, RNA was extracted from the supernatant using the
741 Zymo DirectZOL kit (Zymo Research) following the manufacturer's instructions.

742 Embryo nuclei isolation was performed largely as described in (70). 50-100µl packed embryos were
743 resuspended in 1mL cold buffer 1 (1M sucrose, 1M Tris pH 7.5, 1M $MgCl_2$, 100% Triton X-100, 100mM EGTA, 1M
744 DTT, 1x PTase inhibitor cocktail Roche, 20U/µl SUPERase In Ambion, 1M $CaCl_2$), dounced in a 1m dounce
745 homogenizer with a loose pestle 25 times, centrifuged at 900g for 2 min at 4°C to remove large debris, and
746 dounced again with a tight pestle 15 times on ice. Nuclei were pelleted at 800g for 10 min at 4°C and washed
747 twice in buffer 1 and once in freezing buffer (1M Tris pH 8, 100% glycerol, 100mM $MgAc_2$, 0.5M EDTA, 1M DTT,
748 1x PTase inhibitor cocktail Roche, 20U/µl SUPERase In Ambion). Nuclei were resuspended in freezing buffer,
749 flash-frozen, and stored at -80°C until use.

750

751 **Nuclei and RNA isolation from larval brains for PRO-seq and RNA-seq**

752 Wandering larvae (3rd instar; OreR stock for PRO-seq and iso-1 for RNA-seq) were washed and dissected in
753 PBS. Approximately 125 brains were dissected, flash frozen in liquid nitrogen, and stored at -80°C. Nuclei
754 isolation was performed as described for the embryos but using a 0.5ml dounce homogenizer. Total RNA
755 extraction was performed as described for embryos.

756

757 **PRO-seq library generation, pre-processing and alignment**

758 PRO-seq libraries were prepared as previously described (40). 0.9-4.5 x 10^6 nuclei were mixed with
759 permeabilized 1 x 10^6 Hela nuclei (as spike-in) in 4-biotin-NTP run-on reactions. Run-on RNA was then base-
760 hydrolyzed for 20 min on ice and enriched using M280 streptavidin beads and TRIzol extraction. After
761 amplification, libraries were purified by polyacrylamide gel electrophoresis (PAGE) to remove adapter-dimers
762 and to select molecules below 650 bp in size. Libraries were then sequenced on an Illumina NextSeq 500/550,
763 producing paired-end 100bp reads. We obtained approximately 71 million reads (0-12h embryos) and 55 million
764 reads (L3 brains).

765 Raw fastq files were first trimmed for quality (q 20), length (20 bp), and adapter sequences removed using
766 cutadapt (71). For use with Bowtie 2 (72), paired-end reads were aligned to a combined Human (GRCh38) -
767 *Drosophila* heterochromatin-enriched assembly (24) using default "best match" parameters. A position sorted
768 bam file containing reads mapping to *Drosophila* was de-duplicated (removal of duplicate reads) using Picard's
769 MarkDuplicates (http://broadinstitute.github.io/picard/). It should be noted that read duplicates can emerge
770 during library preparation via PCR, but in the case of PRO-seq they can also be the result of RNA polymerase
771 pausing; since we cannot be sure which is the case with this method, we opted to remove duplicate reads to be
772 conservative. This de-duplicated bam was then processed into a bed file using BEDtools (Quinlan and Hall, 2010),
773 which was used for generation of a 3 'end only (RNA polymerase occupancy position) bed file. This 3 'end only
774 bed file was then used for either: 1) counting read abundance and coverage with BEDtools, or 2) BigWig file
775 generation for visualization in the Integrated Genome Viewer (IGV) (Robinson et al., 2011).

776 For use with Bowtie, read 1 was reverse-complemented using the fastx-toolkit
777 (*http://hannonlab.cshl.edu/fastx_toolkit*) and then aligned to a combined Human (GRCh38) - *Drosophila*
778 heterochromatin-enriched assembly using k-100 parameters (reporting up to 100 mapped loci for each read).
779 Since the purpose of this mapping method was to include multi-mappers as a representation of the "upper
780 bounds" of transcription, de-duplication was not performed on the k-100 read set. Sorted bam files containing
781 reads mapping to *Drosophila* were processed into bed files using BEDtools (73), which were used for either: 1)
782 unique 21-mer filtering (described below in "Meryl unique k-mer filtering"), or 2) generation of 3 ʼend only (RNA
783 polymerase occupancy position) bed files. In the case of option 2) these 3 ʼend only bed files were then use for
784 either: 1) counting read abundance and coverage with BEDtools, or 2) BigWig file generation for visualization in
785 the Integrated Genome Viewer (IGV) (74).

786

787 **RNA-seq library generation, pre-processing, and alignment**

788 RNA-seq libraries were generated using 200ng of RNA from 0-12h embryos or 3rd instar larval brains using
789 Illumina stranded total RNA prep, with the ligation performed with Ribo-Zero Plus and sequenced on Illumina
790 TruSeq Stranded total RNA library prep kit, producing 150bp paired-end reads. We obtained approximately 46
791 million reads (0-12h embryos) and 33 million reads (L3 brains).

792 Raw fastq files were first trimmed for quality (q 20) and length (100 bp), and then adapter sequences
793 removed using cutadapt (71) before being aligned to a *Drosophila* heterochromatin-enriched assembly (24) as
794 paired-end reads using either Bowtie 2 (72) default "best match" parameters or Bowtie k-100 (75). HeLa spike-
795 ins were not included in RNA-seq data and therefore, did not need to be removed. In each case, sorted bam files
796 were processed into bed files using BEDtools (73), which were used for one of the following: 1) unique 51-mer
797 filtering, 2) counting read abundance and coverage with BEDtools, or 3) BigWig file generation (BEDtools,
798 GenomeBrowser/20180626) for visualization in the Integrated Genome Viewer (IGV) (74).

799

800 **Meryl unique k-mer filtering**

801 Single copy k-mers were generated from *Drosophila* heterochromatin-enriched assembly using Meryl (76).
802 We chose the length of single-copy k-mers (21 versus 51-mers) to use for filtering based on the length of the
803 library insert, which is smaller for PRO-seq than for RNA-seq. Bed files of the mapped reads were used to filter
804 through Meryl single copy k-mers using overlapSelect with the option '-overlapBases=XXbp ʼ(XX represents the
805 length of the single copy k-mers (21-mer or 51-mer); GenomeBrowser/20180626). This locus-level filtering
806 requires a minimum of the entire length of k-mer should overlap with a given read in order to be retained. The
807 bed files from all RNA-seq mapping methods (default, k-100, and k-100 51-mer filtered) were used for read
808 counts for repeats and BigWig file generation of IGV visualization (74). The bed files from all PRO-seq mapping
809 methods (default, k-100, and k-100 21-mer filtered) were first processed into 3 ʼend only (RNA polymerase
810 occupancy position) bed files before being used for read counts across repeats and BigWig file generation for
811 IGV visualization.

812

813 **Centromere heat maps for PRO-seq and RNA-seq data**

814 The density of all centromeric repeats was obtained by counting the number of reads mapping to each
815 repeat and dividing it by the number of total reads mapping to that centromeric contig . Read counts of all
816 repeats were obtained with bedtools coverage -counts option. All heatmaps were generated with the ggplot2 R
817 package.

818

819 **CUT&Tag from embryos**

820 2-12h old *Drosophila* iso-1 embryos were collected from cages containing grape-juice agar plates with yeast
821 paste incubated overnight at 25°C. Embryos were washed in embryo wash buffer (0.7% NaCl, 0.04% Triton-
822 X100) and then were dechorionated with 50% bleach for 30s. Embryos were lysed in 1ml buffer B (pH7.5, 15mM
823 Tris-HCl, 15mM NaCl, 60mM KCl, 0.34M Sucrose, 0.5mM Spermidine, 0.1% β-mercaptoethanol, 0.25mM PMSF,
824 2mM EDTA, 0.5mM EGTA) using a homogenizer and filtered through a mesh to remove large debris. Nuclei were
825 spun at 5000g for 5 min and resuspended in 500µl of buffer A (pH7.5, 15mM Tris-HCl, 15mM NaCl, 60mM KCl,
826 0.34M Sucrose, 0.5mM Spermidine, 0.1% β-mercaptoethanol, 0.25mM PMSF) twice. The final pellet was
827 resuspended in CUT&Tag wash buffer (20mM HEPES pH 7.5, 150mM NaCl, 0.5 mM Spermidine) to a final
828 concentration of 1 million nuclei/ml.

829 CUT&Tag was performed on approximately 50,000 nuclei per sample using the pA-Tn5 enzyme from
830 Epycpher, following the manufacturer's instructions (CUT&Tag Protocol v1.5; (46). We used a rabbit anti-
831 Cid/CENP-A antibody (Active Motif cat. 39713, 1:50) and rabbit anti-IgG as negative control (1:100). For the
832 library preparation, we used the primers from (77). Before final sequencing, we pooled 2µl of each library and
833 performed a MiSeq run. We used the number of resulting reads from each library to estimate the relative
834 concentration of each library and ensure an equal representation of each library in the final pool for sequencing.
835 We sequenced the libraries in 150-bp paired-end mode on HiSeq Illumina. We obtained around 6-9 million reads
836 per library, except for the IgG negative control which typically yields much lower reads.

837

838 **CUT&Tag mapping**

839 Raw fastq files of CUT&Tag data were trimmed using trimgalore with these options --paired --nextera --
840 length 35 --phred33 and read quality was assessed with FASTQC. Reads were mapped to Drosophila
841 heterochromatin-enriched assembly with Bowtie2. And MACS2 callpeak was used to call peaks using the IgG as
842 our input control (options -c IgG.bam -f BAMPE -g dm -q 0.01 -B --callsummits). The CENP-A domains were
843 defined based on MACS2 peaks and deepTools bamCompare (78) read coverage. The CENP-A domain for each
844 centromere was determined from the first to the last MACS2 peak. Non-centromeric CENP-A domains were
845 defined based on MACS2 peaks alone without having a single domain for each contig as compared to
846 centromeres. As per Fig. 5B, MACS2 signal intensity values were averaged (BEDtools map -o mean; (73)) from
847 the narrowPeak file across each CENP-A domain.

848

849 **Statistical tests**

850 All *Jockey-3* sequences were extracted from *Drosophila* heterochromatin-enriched assembly annotations
851 using BEDtools (73) and labeled as CENP-A-CEN, CENP-A-nonCEN, or nonCENP-A (requiring at least 1bp overlap
852 with MACS2 CENP-A domains) using BEDtools map -o collapse. *Jockey-3* copies were also labeled as either full-
853 length (FL; if containing a full ORF2) or truncated. Lastly, *Jockey-3* copies were categorized by age based on their
854 divergence from the *Jockey-3* consensus sequence from (61), wherein less than 1% divergence was categorized
855 as 'young' and greater than or equal to 1% was categorized as 'old' (61). It should be noted that the age
856 categorization from Hemmer et al. (61)was available for 326 out of the 329 copies included in all our other
857 analyses. PRO-seq read counts were obtained with BEDtools coverage -counts (requiring at least 1bp overlap)
858 for all *Jockey-3* copies in the genome, as well as for each CENP-A domain and CENP-A-nonCEN-sized random
859 interval. Unique 21-mer coverage per *Jockey-3*, as well as *Jockey-3* coverage per CENP-A domain was assessed
860 using BEDtools coverage. Unpaired *t* tests were performed to quantify differences and determine significance.
861 Scatter box plots and bar graphs were generated via GraphPad Prism (v10.1.1). Heatmaps representing PRO-seq

transcriptional profiles were generated with deepTools computeMatrix and plotHeatmap (Ramirez et al., 2016). Specific plotting parameters include: --averageTypeBins max, --averageTypeSummaryPlot mean, and --zMax 9.

Code and data access

All code for analyses and figures are available on Github https://github.com/bmellone/Dmel-Centromere-Transcription. All sequencing data is available on NCBI under Bioproject PRJNA1082342.

Figure legends:

Figure 1. The transcriptional profile of Drosophila centromeres reveals Jockey-3 as a major transcribed element

A PRO-seq, RNA-seq signals for 0-12h embryos across all *D. melanogaster* centromeres. Top track shows sense, bottom, antisense. Tracks show read coverage with three mapping methods: Bowtie 2 default "best match" ("lower bounds"; yellow), over-fit ("upper bounds"; gray) and a filtered over-fit ("intermediate bounds"; blue). For PRO-seq we used Bowtie k-100 for over-fit, and Bowtie k-100 unique 21-mer filtered for intermediate bounds. For RNA-seq we used Bowtie2 k-100 for over-fit and Bowtie2 k-100 unique 51-mer filtered for intermediate bounds. Repeat annotation is shown on top (see legend for details), with unique 21 and 51-mers (black) used for the filtering shown below. The k-mer tracks illustrate the regions that lack sequence specificity and are therefore most prone to read loss through k-mer filtering. Coordinates shown are kilobases. The boundaries of centromere islands are demarcated by a red dashed line.

B PRO-seq read density scatter boxplot comparison between full-length and truncated (minus three outliers) *Jockey-3* copies, regardless of genome location. Mapping was done with Bowtie 2 default "best match" using paired-end reads, post-deduplication. An unpaired t-test determined a statistically significant difference (****; $p < 0.0001$; Student's t-test). Standard deviation error bars are shown.

C PRO-seq read density scatter-boxplot comparisons of centromeric *Jockey-3* copies split by chromosome and whether they are full-length vs. truncated. Since chromosome Y includes both full-length and truncated copies, a third bar was included encompassing all copies; all three bars are indicated by a dashed box. Mapping was performed with Bowtie 2 default "best match" using paired-end reads, post-deduplication. FL, full-length, Trunc, truncated. Note that only the Y centromere contains FL copies, hence for all other centromeres 'All' is made up of only truncated copies. An unpaired t-test determined a statistically significant difference (****; $p < 0.0001$; ***, $p < 0.001$; Student's t-test). All other comparisons with Y_FL have $p < 0.0001$ (omitted in plot). Error bars show the standard deviation.

D Left, density plot of all repetitive elements on each candidate centromere contig grouped by type as in Chang et al (non-LTR retroelements, LTR retroelements, rDNA-related sequences, simple satellites, and DNA transposon) using an updated genome annotation from Hemmer et al (61). An * indicates annotations based on similarity to retroelements in other *Drosophila* species: *Jockey-1* and *Gypsy-2* are from *D. simulans*, *Gypsy-24* and *Gypsy-27* are from *D. yakuba*, and *Gypsy-7* is from *D. sechellia*.

Right, density plots showing PRO-seq reads (k-100 filtered) for a given repeat (see label from C) normalized by the total number of reads mapping to each contig. Density scale is shown in blue. Gray indicates zero copies/reads for a given repeat.

903 **Figure 2. *Jockey-3* transcripts localize to metaphase chromosomes**

904 **A** Diagram of *Jockey-3* showing base-pair position, predicted protein domains, and coverage of ORF1 (magents)
905 and ORF2 (teal) probe sets.

906 **B-D** Representative iso-1 male larval brain metaphase spreads. Chromosomes are stained with DAPI (magenta),
907 RNA-FISH for *Jockey-3* ORF2 (B), ORF2 sense (C), and ORF1 (D) probes and IF for CENP-C (green). The images on
908 the left show the merged channels and a grayscale 1.5x zoom inset for the Y centromere. The images on the
909 right show DAPI and RNA FISH signals.

910 **E** Graph for the percent of mitotic chromosomes showing colocalization between CENP-C and *Jockey-3* RNA FISH
911 signal. ORF2 (N=3 brains, n=83 spreads), ORF2 anti (N=3 brains, n=28 spreads), and ORF1 (N=4 brains, n=69
912 spreads).

913 **F** Maximum fluorescence intensity plot of centromeric *Jockey-3* RNA FISH signal. ORF2 probe (N= 1 brain, n=30
914 spreads) and ORF1 (N=1 brain, n=30 spreads). The numbers shown above each bar indicate the number of hits
915 predicted to have complementarity with the corresponding probe set. A.U. stands for arbitrary units.

916

917 **Figure 3. *Jockey-3* transcripts co-localize with their cognate sequences in *cis***

918 **A** Schematic showing the organization of centromere 3 (top) and 2 (bottom) and the number of probes from the
919 ORF1 and the ORF2 (both sense) predicted to bind to the *Jockey-3* elements therein.

920 **B** Representative spread from RNA-FISH/IF in iso-1 flies showing the presence of *Jockey-3* signal for the ORF2
921 (yellow) at the centromere of chromosome 3 (arrowhead) and for the ORF1 (cyan) at the centromere of
922 chromosome 2. CENP-C (green) and DNA stained with DAPI (magenta). Bar 1µm.

923 **C** Schematic showing the *de novo* centromere system for chromosome 3 (lacO 3^{peri}). Progeny containing one
924 lacO chromosome 3, UAS-CAL1-GFP-LacI, and elav-GAL4 were analyzed by sequential IF/RNA/DNA FISH.

925 **D** Sequential IF/RNA (left)/DNA-FISH (right) on larval brain metaphase spreads of *de novo* centromere progeny
926 (CAL1-GFP-LacI; lacO 3^{peri}) showing *Jockey-3* transcripts (3 ’probe; yellow) overlapping with the endogenous
927 centromere 3 (yellow arrowhead) but not the *de novo* centromere on lacO (asterisk). CENP-C is a centromere
928 marker (green), *dodeca* is a satellite specific for centromere 3 (cyan). The lacO array DNA FISH is shown in yellow
929 in the right panel. Bar 1µm. N=6 brains (3 males, 3 females), n=90 cells total.

930

931 **Figure 4. Knockdown of *Jockey-3* RNA does not negatively affect normal centromere function**

932 **A** Table showing centromeric and non-centromeric *Jockey-3* copies targeted by the sh-*Jockey-3* over the total
933 number of *Jockey-3* copies. Targets with up to 3 mismatches are included.

934 **B** Efficiency of *Jockey-3* knockdown determined by RT-qPCR normalized to Rp49 and set relative to sh-mcherry
935 control in elav-GAL4 male larval brains. The average of three biological replicates are shown. The primers used
936 here capture 72/329 (ORF2 RT primer set) *Jockey-3* copies throughout the genome and 72/80 targeted by the
937 sh, 32 of which are centromeric copies (two on X, 27 on the Y, 2 on the 3rd, and 3 on 4th chromosome).

938 **C** Representative images of mitotic spreads from larval brains expressing sh-mcherry control and sh-*Jockey-3*
939 stained by IF/RNA-FISH with CENP-C antibodies (green) and *Jockey-3* ORF1 (cyan) and ORF2 (yellow) probes.
940 Insets show a zoomed image of the centromeres in the box. Bar 1µm.

941 **D** Quantification of *Jockey-3* ORF2 and ORF2 RNA-FISH signals at the Y centromere. Bar graphs show the average
942 fluorescence intensity for *Jockey-3* ORF2 and ORF1 at the Y centromere from sh-mcherry and sh-*Jockey-3*

943 (unpaired t-test, p>0.05 for both the *Jockey-3* ORF2 and ORF2, N=3 brains, n=25 Y centromeres/brain). A.U.
944 stands for arbitrary units.

945 **E** Quantification of CENP-C signals at the Y centromere. The bar graph shows the average fluorescence intensity
946 for CENP-C at the Y centromere from sh-mcherry and sh-*Jockey-3* (unpaired t-test, p>0.05, N=3 brains, n=25 Y
947 centromeres/brain). A.U. stands for arbitrary units.

948 **F** Quantification of *Jockey-3* ORF2 and ORF2 RNA-FISH signals in the total interphase cell nucleus. Bar graphs
949 show the average fluorescence intensity for *Jockey-3* ORF2 and ORF1 in the cell nucleus from sh-mcherry and
950 sh-*Jockey-3*. (unpaired t-test, p>0.05 for both *Jockey-3* ORF2 and ORF2, N=3 brains, n=25 Y centromeres/brain).
951 A.U. stands for arbitrary units.

952

953 **Figure 5. Relationship between CENP-A occupancy and transcription at centromeric and non-centromeric**
954 ***Jockey-3* insertions**

955 **A** Scatter boxplot showing CENP-A domain size (in base pairs) between centromeric (n=5) and non-centromeric
956 (n=333) loci based on MACS2 peak calls from CUT&Tag data. Statistical significance was determined with
957 unpaired t-test (****; p < 0.0001; Student's t-test). Error bars show the standard deviation .

958 **B** Scatter boxplot showing CENP-A peak signal intensity between centromeric and non-centromeric loci based on
959 MACS2 peak calls from CUT&Tag data. Signal intensity was averaged across each CENP-A domain. Statistical
960 significance was determined with unpaired t-test (****; p < 0.0001; Student's t-test). Error bars show the
961 standard deviation.

962 **C** Bar graph illustrating the proportion of *Jockey-3* copies expressed per group, where groups are based on
963 CENP-A and centromeric association. PRO-seq mapping was done with Bowtie 2 default "best match" using
964 paired-end reads, post-deduplication. Expression is defined as having at least two PRO-seq read overlaps.

965 **D** Same as shown in **C**, except *Jockey-3* copies found within CENP-A domains (regardless of centromeric
966 association) are combined into one group ("CENP-A").

967 **E** Distribution of *Jockey-3* copies as a stacked bar graph. Copies are grouped by whether they are found within
968 CENP-A domains (regardless of centromeric association) or outside CENP-A domains, as well as their status as a
969 full-length (blue) or truncated elements (gray).

970 **F** PRO-seq read density scatter boxplot of full-length *Jockey-3* copies comparing those found within CENP-A
971 domains (centromeric and non-centromeric) and those found outside CENP-A domains. Mapping was done with
972 Bowtie 2 default "best match" using paired-end reads, post-deduplication. Statistical significance was
973 determined with unpaired t-test (****; p < 0.0001). Error bars show the standard deviation.

974 **G** Same as shown in **F**, except full-length *Jockey-3* copies found within CENP-A domains are split by centromeric
975 (present only within the Y centromere) or non-centromeric locations. Unpaired t-tests (Student's t-test) were
976 performed between each group (***, p < 0.001; ns (non-significant), p > 0.05). Error bars show the standard
977 deviation.

978

979 **Figure 6. Recent *Jockey-3* insertions are found more frequently within CENP-A chromatin and are more**
980 **expressed**
981 **A** Percentage of young *Jockey-3* copies (<1% divergence from consensus) found within CENP-A domains,
982 designated as centromeric (CEN) and non-centromeric (non-CEN), versus non-CENP-A regions identified by
983 CUT&Tag. 61% of young insertions (21/34) are at non-centromeric CENP-A domains (non-CEN) compared to 38%
984 (13/34) centromeric (CEN).

985 **B** PRO-seq read counts mapping to young versus old Jockey-3 copies with Bowtie 2 default "best match", post-
986 deduplication (****, p<0.0001, unpaired t-test).
987
988 **Figure 7. *lacO* transcription is coupled with *de novo* centromere formation**
989 **A** Sequential IF/RNA/DNA FISH on larval brains from GFP-LacI and CAL1-GFP-LacI/3^{peri}, both (lacO array at 3^{peri}).
990 IF for CENP-C is shown in green. RNA and DNA FISH with a lacO LNA probe are shown in yellow. DNA FISH for
991 *dodeca* is shown in cyan.
992 **B** Bar graphs showing the frequency of lacO transcription in GFP-LacI and CAL1-GFP-LacI/3^{peri} in metaphase and
993 **C** in interphase (Fisher's exact test, N = 5 brains, n = 15 spreads/brain).
994 **D** Scatter plot showing the fluorescence intensity of lacO RNA-FISH in GFP-LacI and CAL1-GFP-LacI/3^{peri} in
995 metaphase (nested t-test, N = 3 brains, n = 6-11 spreads/brain). A.U. stands for arbitrary units.
996

997 **Supplemental Figure Legends**

998 **Figure S1: PRO-seq reads aligned to genes show expected enrichment of RNA polymerase occupancy at gene**
999 **promoters.** Heatmaps of RNA polymerase occupancy mapped using Bowtie 2 default "best match" for antisense
1000 (blue) and sense (red) strands per gene. Composite profiles (line graphs) across all genes are shown along the
1001 top.

1002 **A** All genes are anchored to the 5 'end (transcription start site (TSS)) with a specified distance into the gene body
1003 denoted in the bottom right (2.5kb), and a specified distance away from the gene body denoted in the bottom
1004 left (0.5kb). The dotted line per heatmap denotes the static end of each gene as they are sorted longest to
1005 shortest from top to bottom. This highlights the anticipated enrichment of RNA polymerase at the promoter.

1006 **B** All genes are scaled to the same size with a specified distance on either side of the gene body denoted in the
1007 bottom corners (0.1kb). The genes are included in the heatmap based on transcriptional signal intensity from
1008 top to bottom. This highlights RNA polymerase activity across the entire gene, with an enrichment at the
1009 promoter, reduction over the gene body, and a slight enrichment at the 3 'end indicative of polymerase slow-
1010 down as termination occurs.

1011 **C** Same as shown in **A**, except using PRO-seq reads that have been deduplicated. This highlights the overall
1012 preservation of the transcriptional pattern following deduplication with an expected loss of reads,
1013 predominantly at the promoter since this is where polymerase density naturally highest, meaning duplicate
1014 reads are more likely at this position.

1015 **D** Same as shown in **B**, except using PRO-seq reads that have been deduplicated. This highlights the overall
1016 preservation of the transcriptional pattern following deduplication with an expected loss of reads at the
1017 promoter as well as at the 3 'end where termination is occurring.

1018

1019 **Fig. S2: FL vs truncated k-100 and k-100 filtered PRO-seq**

1020 **A** PRO-seq read density scatter boxplot comparisons between full-length (FL) and truncated *Jockey-3* copies,
1021 regardless of genome location. Mapping was done with Bowtie k-100 and k-100 21-mer filtered using single-end
1022 reads. Unpaired t-tests (Student's t-test) were performed indicating a significant difference (****, p < 0.0001)
1023 between each group illustrating a consistent trend seen across all three mapping methods (Fig. 1B). Standard
1024 deviation error bars are shown.

1025 **B** Meryl unique 21-mer coverage for FL and truncated *Jockey-3* copies. An unpaired t test (Student's t-test) was
1026 performed indicating a significant difference (****, p < 0.0001), wherein truncated copies have more unique 21-
1027 mers as a result of having accumulated more mutations over time making them less similar to each other.

1028

1029 **Fig. S3: PRO-seq and RNA-seq from larval brains.** PRO-seq, RNA-seq signals for 3rd instar larval brains across all
1030 *D. melanogaster* centromeres. Top track shows sense, bottom, antisense. Tracks show read coverage with three
1031 mapping methods: Bowtie 2 default best match ("lower bounds"; yellow), over-fit ("upper bounds"; gray) and a
1032 filtered over-fit ("medium bounds"; blue). For PRO-seq we Bowtie1 k-100 for over-fit, and Bowtie1 k-100 21-mer
1033 filtered for medium bounds. For RNA-seq we used Bowtie2 k-100 for over-fit and Bowtie2 k-100 51-mer filtered
1034 for medium bounds. Repeat annotation is shown on top (see legend for details), with unique 21 and 51-mers
1035 (black) used for the filtering shown below. The k-mer tracks illustrate the regions that lack sequence specificity
1036 and are therefore most prone to read loss through k-mer filtering. Coordinates shown are kilobases. Dotted red
1037 line indicates the boundaries of the islands.

1038

1039 **Figure S4: RNA-FISH detects the chromosome-associated non-coding RNA *Rox1*.** RNA-FISH/IF on *D.*
1040 *melanogaster* (iso-1) mitotic chromosomes from male larval brains with the ORF2 of *Jockey-3* probe (yellow), a
1041 *Rox1* probe (cyan), and with CENP-C antibodies (green). DNA is stained with DAPI (magenta). Bars 1µm. Arrow
1042 points to *Rox1* (yellow) localization on the arms of the X chromosome.

1043

1044 **Figure S5: *Jockey-3* RNA localization on centromeres of individual chromosomes.** RNA-FISH/IF on *D.*
1045 *melanogaster* (iso-1) mitotic chromosomes from male larval brains. Individual chromosomes showing
1046 centromeric signal for each *Jockey-3* probe set (ORF2, ORF2 anti, and ORF1) (yellow) on chromosomes (X, Y, 2, 3,
1047 and 4), CENP-C showing the centromere (green), and DAPI (magenta). Insets show CENP-C and *Jockey-3* signals.
1048 Bars 1µm

1049

1050 **Figure S6 *Jockey-3* RNA localizes to mitotic centromeres in other tissues and in *D. simulans***

1051 **A** RNA-FISH/IF on mitotic chromosomes from *D. melanogaster* (iso-1) adult ovaries. IF for CENP-C (green) and
1052 RNA-FISH for *Jockey-3* ORF2 (yellow). DNA is stained with DAPI (magenta).

1053 **B** RNA-FISH/IF on mitotic spreads from S2 cells. IF for CENP-C (green), and RNA-FISH for *Jockey-3* ORF2 (yellow)
1054 and SatIII (found on X and 3rd chromosomes; cyan). DNA is stained with DAPI (magenta).

1055 **C** RNA-FISH/IF on *D. simulans* (laboratory stock w501) mitotic chromosomes from male larval brains. IF with
1056 CENP-C (green) and RNA-FISH for *Jockey-3* ORF2 and *Rox1* (stains the X, control; cyan). DNA is stained with DAPI
1057 (magenta). Bar 1µm

1058

1059 **Figure S7: RNA foci detected with *Jockey-3* ORF2 correspond to RNA, not DNA**

1060 **A** RNA-FISH on *D. melanogaster* (iso-1) mitotic chromosomes from male larval brains for the 3 ʾsense of *Jockey-3*
1061 (yellow) and an OligoPaint for 61C7 (green). Green arrow indicates presence of signal, white arrow indicates lack
1062 of signal.

1063 **B** DNA-FISH on *D. melanogaster* (iso-1) mitotic chromosomes from male larval brains with stellaris FISH probes
1064 for ORF2 of *Jockey-3* (yellow) and an OligoPaint for 61C7 (green). Green arrow indicates presence of signal,
1065 white arrow indicates lack of signal. Bars 5µm.

1066

1067

1068 **Figure S8: RNase treatments result in a decrease in *Jockey-3* RNA-FISH signal**

1069 **A** RNA-FISH with *Jockey-3* ORF2 on *D. melanogaster* male larval brain monolayers expressing eCENP-A-EGFP
1070 (green). DNA is stained with DAPI (magenta). Shown are the before and after treatments with and without
1071 RNase H.

1072 **B** Quantification of the number of ORF2 *Jockey-3* foci before and after RNase H treatment (not significant for
1073 before and p<0.0001 for after treatment). Quantification of the number of eCENP-A-EGFP foci before and after
1074 RNase H treatment (p=0.367 for before and not significant for after treatment). N=1 brain, n=107 cells
1075 quantified for before treatment and n=86 cells for after treatment).

1076 **C** RNA-FISH with *Jockey-3* ORF2 and *Rox1* (cyan; control) on *D. melanogaster* male larval brain monolayers
1077 expressing eCENP-A-EGFP (under the endogenous CENP-A promoter; green).

1078 **D** Quantification of eCENP-A-GFP (N=1 brain, n=100 cells; *p = 0.0292*)* and ORF2 *Jockey-3* foci (N=1 brain, n=100
1079 cells; ****p = <0.0001)*.*

1080

1081 **Figure S9: Quantification of non-centromeric *Jockey-3* foci in mitotic cells.** Graph showing the non-centromeric
1082 localization of *Jockey-3* (ORF2, ORF2 anti, and ORF1) on mitotic chromosomes from larval brain squashes. XR, 4L,
1083 and 4R were not quantified since these arms are cytologically too small and too close to the centromeres to be
1084 distinguished. ORF2 (N=3 brains, n=83 spreads), ORF2 anti (N=3 brains, n=28 spreads), and ORF1 (N=4 brains,
1085 n=69 spreads).

1086

1087 **Figure S10: RNA-FISH *Jockey-3* foci are present during interphase**

1088 **A** RNA-FISH/IF with ORF2 (yellow) and ORF1 (magenta) *Jockey-3* probes and CENP-C (green) on interphase cells
1089 from male larval brain squashes.

1090 **B** IF/RNA-FISH as in A on S2 cells (30% of cells have at least 1 co-localizing CENP-C/*Jockey-3* spot, n=54; note that
1091 S2 cells do not have a Y chromosome).

1092 **C** RNA-FISH/IF as in A on ovary squashes. Insets show magnification of centromeres in the box.

1093 **D** Graph showing the average number of *Jockey-3* ORF2 foci that co-localize with CENP-C (cen) versus not (non-
1094 cen).

1095 **E** Graph of the average number of centromeric *Jockey-3* foci in interphase versus metaphase cells. N=3 brains,
1096 n=30-105 cells per brain.

1097 **F** Graph showing the % of cells showing 2 or more *Jockey-3* foci co-localizing with CENP-C in interphase versus
1098 mitosis. Data in **D-F** is all from the same 3 male larval brains as in **A**.

1099

1100 **Figure S11: RNA-FISH for centromeric retroelement *Doc*.** RNA-FISH/IF on *D. melanogaster* (iso-1) male larval
1101 brain squashes. Immunofluorescence for CENP-C (green), and RNA-FISH for *Jockey-3* ORF2 (yellow) and *DOC*
1102 sense (cyan). *Doc* is present in the islands of centromere X and 4. Dashed box shows the X centromere lacking
1103 *Doc* signal. The solid line box shows a centromere with *Doc* signal in interphase. DNA is stained with DAPI
1104 (magenta).

1105

1106 **Figure S12: IGV tracks for CENP-A CUT&Tag.** IGV tracks showing CUT&Tag signals for 0-12h embryos across all *D.*
1107 *melanogaster* centromeres. Top track shows color-coded repeat annotation (details in legend). CUT&Tag track

1108 shows CENP-A enrichment in gray. Red dotted line shows the span of the CENP-A domain we defined for each
1109 centromere. Predicted MACS2 peaks for CUT&Tag data are shown in bottom track (black).

1110

1111 **Figure S13: CENP-A associated k-100 and k-100 filtered PRO-seq.**

1112 **A** Bar graph illustrating the proportion of CENP-A associated *Jockey-3* copies expressed within the centromere
1113 and outside the centromere. PRO-seq mapping was done with Bowtie k-100 and k-100 21-mer filtered using
1114 single-end reads. Expression is defined as having at least two PRO-seq read overlaps. The trend difference seen
1115 between Bowtie 2 default and Bowtie k-100 methods can be attributed to the lower unique 21-mer coverage of
1116 CENP-A copies allowing more reads to map to these copies.

1117 **B** Meryl unique 21-mer coverage for CENP-A associated *Jockey-3* copies based on centromeric loci designation.
1118 Unpaired t tests (Student's t-test) were performed indicating a significant difference (****, $p < 0.0001$; ***, $p <$
1119 0.001; ns (non-significant), $p > 0.05$) between each group. Standard deviation error bars are shown.

1120

1121 **Supplemental Table Legends**

1122 **Table S1: PRO-seq read and unique 21-mer coverage across all *Jockey-3* loci.** Table showing all 329 *Jockey-3*
1123 copies per CENP-A and centromeric association further distinguished by age based on divergence from
1124 consensus (<1%). PRO-seq read coverage for all three mapping methods are included: Bowtie 2 default "best
1125 match" using paired-end reads (post-deduplication), and Bowtie k-100 and Bowtie k-100 21-mer filtered, both
1126 using single-end reads. Coverage of Meryl unique 21-mers per copy is also shown. Data included was used for
1127 **Figs. 1B-C**, **Figs. 5F-G, Figs. S2 and S13, and Fig. 6**. Note: This table includes three truncated, old nonCENP-A
1128 copies indicated by an asterisk (*) in columns E & F, which are included in all analyses except those represented
1129 in **Fig. 6**.

1130 **Table S2: Read counts for heatmaps.** Table showing the PRO-seq read count for each centromeric repeat within
1131 all centromere contigs. This data was used to generate the heatmaps shown in **Fig. 1**.

1132 **Table S3: *Jockey-3* RNA-FISH probe sequences mapped across the genome.** The table shows the chromosome,
1133 contig, and coordinates of every *Jockey-3* copy in the genome. The first tab shows just the full-length copies, the
1134 second shows all the centromeric and the last all non-centromeric insertions. Indicated are the type of
1135 chromatin they are found in (if known; designated as in (24)), approximate cytological location and number of
1136 probes predicted to bind. This information was used for the graph in **Fig. 2F**.

1137 **Table S4: CENP-A domain loci, both centromeric and non-centromeric.** Table showing all five centromeric and
1138 333 non-centromeric CENP-A domains as defined by MACS2 peak calls from CUT&Tag data. Size (basepairs),
1139 average MACS2 peak signal intensity, and PRO-seq read overlap is shown per CENP-A domain. PRO-seq mapping
1140 was done with Bowtie 2 default "best match" using paired-end reads, post-deduplication. Data included was
1141 used for **Figs. 5A-B.**

1142 **Table S5: Proportion of *Jockey-3* copies expressed based on PRO-seq read overlap.**

1143 **A** Table showing the number of *Jockey-3* copies (FL and truncated) expressed per CENP-A and centromeric
1144 association. Expression is defined as having at least two PRO-seq read overlaps. All three mapping methods are
1145 included: Bowtie 2 default "best match" using paired-end reads (post-deduplication), and Bowtie k-100 and
1146 Bowtie k-100 21-mer filtered, both using single-end reads. Data included (representing 329 copies) was used for
1147 **Figs. 5C-D and Fig. S13.**

1148 **B** Same as shown in **A**, except further distinguished by age based on divergence from consensus (<1%) and only
1149 representing the 326/329 copies with age distinctions (young vs. old). Data included was used for **Fig. 6**.

1150 **Table S6: Summary of CENP-A-associated truncated and full-length (FL) *Jockey-3* insertions.** Table showing the
1151 distribution of all 329 *Jockey-3* copies associated with CENP-A and/or centromeres across the genome. A column
1152 for other repeats, excluding *Jockey-3*, is shown to emphasize the enrichment of *Jockey-3* associated with CENP-
1153 A. Note: this list does include 3 truncated, old nonCENP-A copies indicated by an asterisk (*), which are include
1154 in all analyses except those represented in Figure 6. Data included was used for **Fig. 5E.**

1155 **Bibliography**

1156

1157 1. Palmer DK, O'Day K, Wener MH, Andrews BS, Margolis RL. A 17-kD centromere protein (CENP-A) copurifies
1158 with nucleosome core particles and with histones. J Cell Biol. 1987;104(4):805-15.

1159 2. Heterochromatic deposition of centromeric histone H3-like proteins, (2000).

1160 3. McKinley KL, Cheeseman IM. The molecular basis for centromere identity and function. Nat Rev Mol Cell
1161 Biol. 2016;17(1):16-29.

1162 4. Marshall OJ, Chueh AC, Wong LH, Choo KH. Neocentromeres: new insights into centromere structure,
1163 disease development, and karyotype evolution. Am J Hum Genet. 2008;82(2):261-82.

1164 5. Ventura M, Antonacci F, Cardone MF, Stanyon R, D'Addabbo P, Cellamare A, et al. Evolutionary formation
1165 of new centromeres in macaque. Science. 2007;316(5822):243-6.

1166 6. Ohkuni K, Kitagawa K. Endogenous transcription at the centromere facilitates centromere activity in
1167 budding yeast. Curr Biol. 2011;21(20):1695-703.

1168 7. Hedouin S, Logsdon GA, Underwood JG, Biggins S. A transcriptional roadblock protects yeast centromeres.
1169 Nucleic Acids Res. 2022;50(14):7801-15.

1170 8. Quenet D, Dalal Y. A long non-coding RNA is required for targeting centromeric protein A to the human
1171 centromere. eLife. 2014;3:e03254.

1172 9. McNulty SM, Sullivan LL, Sullivan BA. Human Centromeres Produce Chromosome-Specific and Array-
1173 Specific Alpha Satellite Transcripts that Are Complexed with CENP-A and CENP-C. Dev Cell. 2017;42(3):226-
1174 40 e6.

1175 10. Bury L, Moodie B, Ly J, McKay LS, Miga KH, Cheeseman IM. Alpha-satellite RNA transcripts are repressed by
1176 centromere-nucleolus associations. eLife. 2020;9.

1177 11. Hoyt SJ, Storer JM, Hartley GA, Grady PGS, Gershman A, de Lima LG, et al. From telomere to telomere: The
1178 transcriptional and epigenetic state of human repeat elements. Science. 2022;376(6588):eabk3112.

1179 12. Blower MD. Centromeric Transcription Regulates Aurora-B Localization and Activation. Cell Rep.
1180 2016;15(8):1624-33.

1181 13. Grenfell AW, Heald R, Strzelecka M. Mitotic noncoding RNA processing promotes kinetochore and spindle
1182 assembly in Xenopus. J Cell Biol. 2016;214(2):133-41.

1183 14. Topp CN, Zhong CX, Dawe RK. Centromere-encoded RNAs are integral components of the maize
1184 kinetochore. Proc Natl Acad Sci U S A. 2004;101(45):15986-91.

1185 15. Carone DM, Zhang C, Hall LE, Obergfell C, Carone BR, O'Neill MJ, et al. Hypermorphic expression of
1186 centromeric retroelement-encoded small RNAs impairs CENP-A loading. Chromosome Res. 2013;21(1):49-
1187 62.

1188 16. Chen CC, Bowers S, Lipinszki Z, Palladino J, Trusiak S, Bettini E, et al. Establishment of Centromeric
1189 Chromatin by the CENP-A Assembly Factor CAL1 Requires FACT-Mediated Transcription. Dev Cell.
1190 2015;34(1):73-84.

1191 17. Chueh AC, Northrop EL, Brettingham-Moore KH, Choo KH, Wong LH. LINE retrotransposon RNA is an
1192 essential structural and functional epigenetic component of a core neocentromeric chromatin. PLoS Genet.
1193 2009;5(1):e1000354.

1194 18. Murillo-Pineda M, Valente LP, Dumont M, Mata JF, Fachinetti D, Jansen LET. Induction of spontaneous
1195 human neocentromere formation and long-term maturation. J Cell Biol. 2021;220(3).

1196 19. Naughton C, Huidobro C, Catacchio CR, Buckle A, Grimes GR, Nozawa RS, et al. Human centromere
1197 repositioning activates transcription and opens chromatin fibre structure. Nat Commun. 2022;13(1):5609.

1198 20. Wu W, McHugh T, Kelly DA, Pidoux AL, Allshire RC. Establishment of centromere identity is dependent on
1199 nuclear spatial organization. Curr Biol. 2022;32(14):3121-36 e6.

1200 21. Bobkov GOM, Gilbert N, Heun P. Centromere transcription allows CENP-A to transit from chromatin
1201 association to stable incorporation. J Cell Biol. 2018.

1202 22. Cardinale S, Bergmann JH, Kelly D, Nakano M, Valdivia MM, Kimura H, et al. Hierarchical inactivation of a
1203 synthetic human kinetochore by a chromatin modifier. Mol Biol Cell. 2009;20(19):4194-204.

1204 23. Rosic S, Kohler F, Erhardt S. Repetitive centromeric satellite RNA is essential for kinetochore formation and
1205 cell division. J Cell Biol. 2014;207(3):335-49.

1206 24. Chang CH, Chavan A, Palladino J, Wei X, Martins NMC, Santinello B, et al. Islands of retroelements are major
1207 components of Drosophila centromeres. PLoS Biol. 2019;17(5):e3000241.

1208 25. Garrigan D, Kingan SB, Geneva AJ, Andolfatto P, Clark AG, Thornton KR, et al. Genome sequencing reveals
1209 complex speciation in the Drosophila simulans clade. Genome Res. 2012;22(8):1499-511.

1210 26. Jagannathan M, Warsinger-Pepe N, Watase GJ, Yamashita YM. Comparative Analysis of Satellite DNA in the
1211 Drosophila melanogaster Species Complex. G3 (Bethesda). 2017;7(2):693-704.

1212 27. Courret C, Hemmer L, Wei X, Patel PD, Santinello B, Geng X, et al. Rapid turnover of centromeric DNA
1213 reveals signatures of genetic conflict in Drosophila. BioRXiv. 2023.

1214 28. Presting GG. Centromeric retrotransposons and centromere function. Curr Opin Genet Dev. 2018;49:79-84.

1215 29. Choi ES, Stralfors A, Castillo AG, Durand-Dubief M, Ekwall K, Allshire RC. Identification of noncoding
1216 transcripts from within CENP-A chromatin at fission yeast centromeres. J Biol Chem. 2011;286(26):23600-7.

1217 30. Chan FL, Marshall OJ, Saffery R, Kim BW, Earle E, Choo KH, et al. Active transcription and essential role of
1218 RNA polymerase II at the centromere during mitosis. Proc Natl Acad Sci U S A. 2012;109(6):1979-84.

1219 31. Chan FL, Wong LH. Transcription in the maintenance of centromere chromatin identity. Nucleic Acids Res.
1220 2012;40(22):11178-88.

1221 32. Choi ES, Stralfors A, Catania S, Castillo AG, Svensson JP, Pidoux AL, et al. Factors that promote H3 chromatin
1222 integrity during transcription prevent promiscuous deposition of CENP-A(Cnp1) in fission yeast. PLoS Genet.
1223 2012;8(9):e1002985.

1224 33. Mellone BG, Fachinetti D. Diverse mechanisms of centromere specification. Curr Biol. 2021;31(22):R1491-
1225 R504.

1226 34. Klein SJ, O'Neill RJ. Transposable elements: genome innovation, chromosome diversity, and centromere
1227 conflict. Chromosome Res. 2018;26(1-2):5-23.

1228 35. Rosic S, Erhardt S. No longer a nuisance: long non-coding RNAs join CENP-A in epigenetic centromere
1229 regulation. Cell Mol Life Sci. 2016;73(7):1387-98.

1230 36. Grenfell AW, Strzelecka M, Heald R. Transcription brings the complex(ity) to the centromere. Cell Cycle.
1231 2017;16(3):235-6.

1232 37. Perea-Resa C, Blower MD. Centromere Biology: Transcription Goes on Stage. Mol Cell Biol. 2018;38(18).

1233 38. Mills WK, Lee YCG, Kochendoerfer AM, Dunleavy EM, Karpen GH. RNA from a simple-tandem repeat is
1234 required for sperm maturation and male fertility in Drosophila melanogaster. eLife. 2019;8.

1235 39. Wei X, Eickbush DG, Speece I, Larracuente AM. Heterochromatin-dependent transcription of satellite DNAs
1236 in the Drosophila melanogaster female germline. eLife. 2021;10.

1237 40. Mahat DB, Kwak H, Booth GT, Jonkers IH, Danko CG, Patel RK, et al. Base-pair-resolution genome-wide
1238 mapping of active RNA polymerases using precision nuclear run-on (PRO-seq). Nat Protoc. 2016;11(8):1455-
1239 76.

1240 41. Hemmer NS, Geng X, Courret C, Navarro-Domínguez B, Speece I, Wei X, Altidor E, Chaffer J, Sproul J,
1241 Larracuente A. Centromere-associated retroelement evolution in Drosophila melanogaster reveals an
1242 underlying conflict. BioRXiv. 2023.

1243 42. Meller VH, Wu KH, Roman G, Kuroda MI, Davis RL. roX1 RNA paints the X chromosome of male Drosophila
1244 and is regulated by the dosage compensation system. Cell. 1997;88(4):445-57.

1245 43. Palladino J, Chavan A, Sposato A, Mason TD, Mellone BG. Targeted De Novo Centromere Formation in
1246 Drosophila Reveals Plasticity and Maintenance Potential of CENP-A Chromatin. Dev Cell. 2020;52(3):379-94
1247 e7.

1248 44. McNulty SM, Sullivan BA. Centromere Silencing Mechanisms. Prog Mol Subcell Biol. 2017;56:233-55.

1249 45. Bassett AR, Akhtar A, Barlow DP, Bird AP, Brockdorff N, Duboule D, et al. Considerations when investigating
1250 lncRNA function in vivo. Elife. 2014;3:e03058.

1251 46. Kaya-Okur HS, Wu SJ, Codomo CA, Pledger ES, Bryson TD, Henikoff JG, et al. CUT&Tag for efficient
1252 epigenomic profiling of small samples and single cells. Nat Commun. 2019;10(1):1930.

1253 47. Nechemia-Arbely Y, Miga KH, Shoshani O, Aslanian A, McMahon MA, Lee AY, et al. DNA replication acts as
1254 an error correction mechanism to maintain centromere identity by restricting CENP-A to centromeres. Nat
1255 Cell Biol. 2019;21(6):743-54.

1256 48. Chen CC, Dechassa ML, Bettini E, Ledoux MB, Belisario C, Heun P, et al. CAL1 is the Drosophila CENP-A
1257 assembly factor. J Cell Biol. 2014;204(3):313-29.

1258 49. Murillo-Pineda M, Jansen LET. Genetics, epigenetics and back again: Lessons learned from neocentromeres.
1259 Exp Cell Res. 2020;389(2):111909.

1260 50. Propagation of centromeric chromatin requires exit from mitosis, (2007).

1261 51. Incorporation of Drosophila CID/CENP-A and CENP-C into centromeres during early embryonic anaphase,
1262 (2007).

1263 52. Mellone BG, Grive KJ, Shteyn V, Bowers SR, Oderberg I, Karpen GH. Assembly of Drosophila centromeric
1264 chromatin proteins during mitosis. PLoS Genet. 2011;7(5):e1002068.

1265 53. Dunleavy EM, Beier NL, Gorgescu W, Tang J, Costes SV, Karpen GH. The cell cycle timing of centromeric
1266 chromatin assembly in Drosophila meiosis is distinct from mitosis yet requires CAL1 and CENP-C. PLoS Biol.
1267 2012;10(12):e1001460.

1268 54. Lidsky PV, Sprenger F, Lehner CF. Distinct modes of centromere protein dynamics during cell cycle
1269 progression in Drosophila S2R+ cells. J Cell Sci. 2013;126(Pt 20):4782-93.

1270 55. Pauleau AL, Bergner A, Kajtez J, Erhardt S. The checkpoint protein Zw10 connects CAL1-dependent CENP-A
1271 centromeric loading and mitosis duration in Drosophila cells. PLoS Genet. 2019;15(9):e1008380.

1272 56. Ranjan R, Snedeker J, Chen X. Asymmetric Centromeres Differentially Coordinate with Mitotic Machinery to
1273 Ensure Biased Sister Chromatid Segregation in Germline Stem Cells. Cell Stem Cell. 2019;25(5):666-81 e5.

1274 57. Dunleavy EM, Almouzni G, Karpen GH. H3.3 is deposited at centromeres in S phase as a placeholder for
1275 newly assembled CENP-A in G(1) phase. Nucleus. 2011;2(2):146-57.

1276 58. Perea-Resa C, Bury L, Cheeseman IM, Blower MD. Cohesin Removal Reprograms Gene Expression upon
1277 Mitotic Entry. Mol Cell. 2020;78(1):127-40 e7.

1278 59. Ghosh S, Lehner CF. Incorporation of CENP-A/CID into centromeres during early Drosophila embryogenesis
1279 does not require RNA polymerase II-mediated transcription. Chromosoma. 2022;131(1-2):1-17.

1280 60. Raychaudhuri N, Dubruille R, Orsi GA, Bagheri HC, Loppin B, Lehner CF. Transgenerational propagation and
1281 quantitative maintenance of paternal centromeres depends on Cid/Cenp-A presence in Drosophila sperm.
1282 PLoS Biol. 2012;10(12):e1001434.

1283 61. Hemmer L, Negm S, Geng X, Courret C, Navarro-Domínguez B, Speece I, et al. Centromere-associated
1284 retroelement evolution in Drosophila melanogaster reveals an underlying conflict. BioRXiv. 2023.

1285 62. Sullivan BA, Karpen GH. Centromeric chromatin exhibits a histone modification pattern that is distinct from
1286 both euchromatin and heterochromatin. Nat Struct Mol Biol. 2004;11(11):1076-83.

1287 63. Jachowicz JW, Bing X, Pontabry J, Boskovic A, Rando OJ, Torres-Padilla ME. LINE-1 activation after
1288 fertilization regulates global chromatin accessibility in the early mouse embryo. Nat Genet.
1289 2017;49(10):1502-10.

1290 64. Limouse C, Smith OK, Jukam D, Fryer KA, Greenleaf WJ, Straight AF. Global mapping of RNA-chromatin
1291 contacts reveals a proximity-dominated connectivity model for ncRNA-gene interactions. Nat Commun.
1292 2023;14(1):6073.

1293 65. Decker CJ, Burke JM, Mulvaney PK, Parker R. RNA is required for the integrity of multiple nuclear and
1294 cytoplasmic membrane-less RNP granules. EMBO J. 2022;41(9):e110137.

1295 66. Rhine K, Vidaurre V, Myong S. RNA Droplets. Annu Rev Biophys. 2020;49:247-65.

1296 67. Schittenhelm RB, Althoff F, Heidmann S, Lehner CF. Detrimental incorporation of excess Cenp-A/Cid and
1297 Cenp-C into Drosophila centromeres is prevented by limiting amounts of the bridging factor Cal1. J Cell Sci.
1298 2010;123(Pt 21):3768-79.

1299 68. Pfaffl MW. A new mathematical model for relative quantification in real-time RT-PCR. Nucleic Acids Res.
1300 2001;29(9):e45.

1301 69. Hanlon SL, Miller DE, Eche S, Hawley RS. Origin, Composition, and Structure of the Supernumerary B
1302 Chromosome of Drosophila melanogaster. Genetics. 2018;210(4):1197-212.

1303 70. Saunders A, Core LJ, Sutcliffe C, Lis JT, Ashe HL. Extensive polymerase pausing during Drosophila axis
1304 patterning enables high-level and pliable transcription. Genes Dev. 2013;27(10):1146-58.

1305 71. Martin M. Cutadapt Removes Adapter Sequences From High-Throughput Sequencing Reads. EMBnet
1306 Journal. 2011;Vol 17, No 1.

1307 72. Langmead B, Salzberg SL. Fast gapped-read alignment with Bowtie 2. Nature methods. 2012;9(4):357-9.

1308 73. Quinlan AR, Hall IM. BEDTools: a flexible suite of utilities for comparing genomic features. Bioinformatics.
1309 2010;26(6):841-2.

1310 74. Robinson JT, Thorvaldsdottir H, Winckler W, Guttman M, Lander ES, Getz G, et al. Integrative genomics
1311 viewer. Nat Biotechnol. 2011;29(1):24-6.

1312 75. Langmead B, Trapnell C, Pop M, Salzberg SL. Ultrafast and memory-efficient alignment of short DNA
1313 sequences to the human genome. Genome Biol. 2009;10(3):R25.

1314 76. Rhie A, Walenz BP, Koren S, Phillippy AM. Merqury: reference-free quality, completeness, and phasing
1315 assessment for genome assemblies. Genome Biol. 2020;21(1):245.

1316 77. Buenrostro JD, Wu B, Chang HY, Greenleaf WJ. ATAC-seq: A Method for Assaying Chromatin Accessibility
1317 Genome-Wide. Curr Protoc Mol Biol. 2015;109:21 9 1- 9 9.

1318 78. Ramirez F, Ryan DP, Gruning B, Bhardwaj V, Kilpert F, Richter AS, et al. deepTools2: a next generation web
1319 server for deep-sequencing data analysis. Nucleic Acids Res. 2016;44(W1):W160-5.

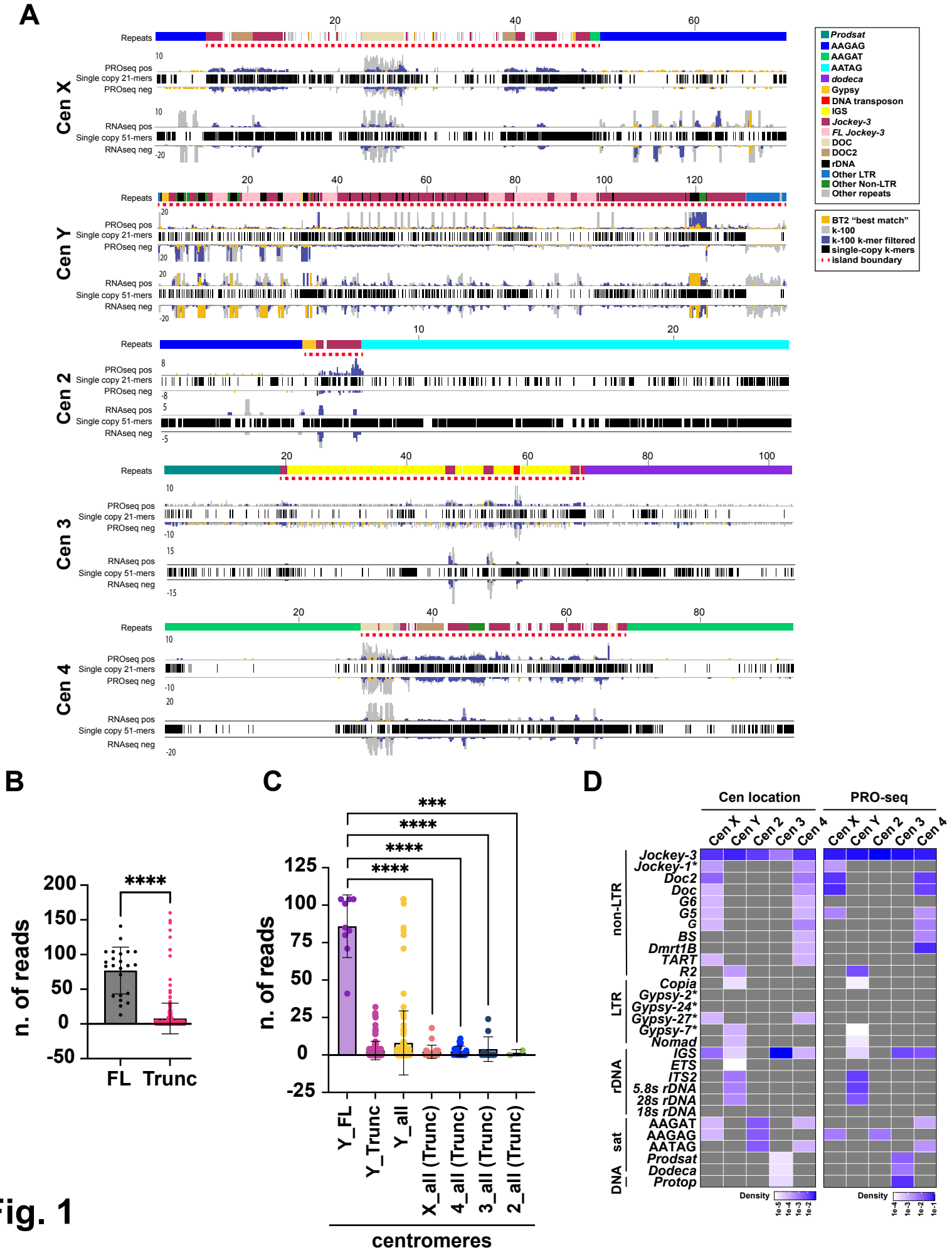
A
Cen X
Cen Y
Cen 2
Cen 3
Cen 4
Repeats
PROseq pos
Single copy 21-mers
PROseq neg
RNAseq pos
Single copy 51-mers
RNAseq neg
Prodsat
AAGAG
AAGAT
AATAG
dodeca
Gypsy
DNA transposon
IGS
Jockey-3
FL Jockey-3
DOC
DOC2
rDNA
Other LTR
Other Non-LTR
Other repeats
BT2 "best match"
k-100
k-100 k-mer filtered
single-copy k-mers
island boundary
B
n. of reads
FL
Trunc
C
n. of reads
Y_FL
Y_Trunc
Y_all
X_all (Trunc)
4_all (Trunc)
3_all (Trunc)
2_all (Trunc)
centromeres
D
Cen location
PRO-seq
Cen X
Cen Y
Cen 2
Cen 3
Cen 4
non-LTR
LTR
rDNA
sat
DNA
Jockey-3
Jockey-1*
Doc2
Doc
G6
G5
G
BS
Dmrt1B
TART
R2
Copia
Gypsy-2*
Gypsy-24*
Gypsy-27*
Gypsy-7*
Nomad
IGS
ETS
ITS2
5.8s rDNA
28s rDNA
18s rDNA
AAGAT
AAGAG
AATAG
Prodsat
Dodeca
Protop
Density

Fig. 1

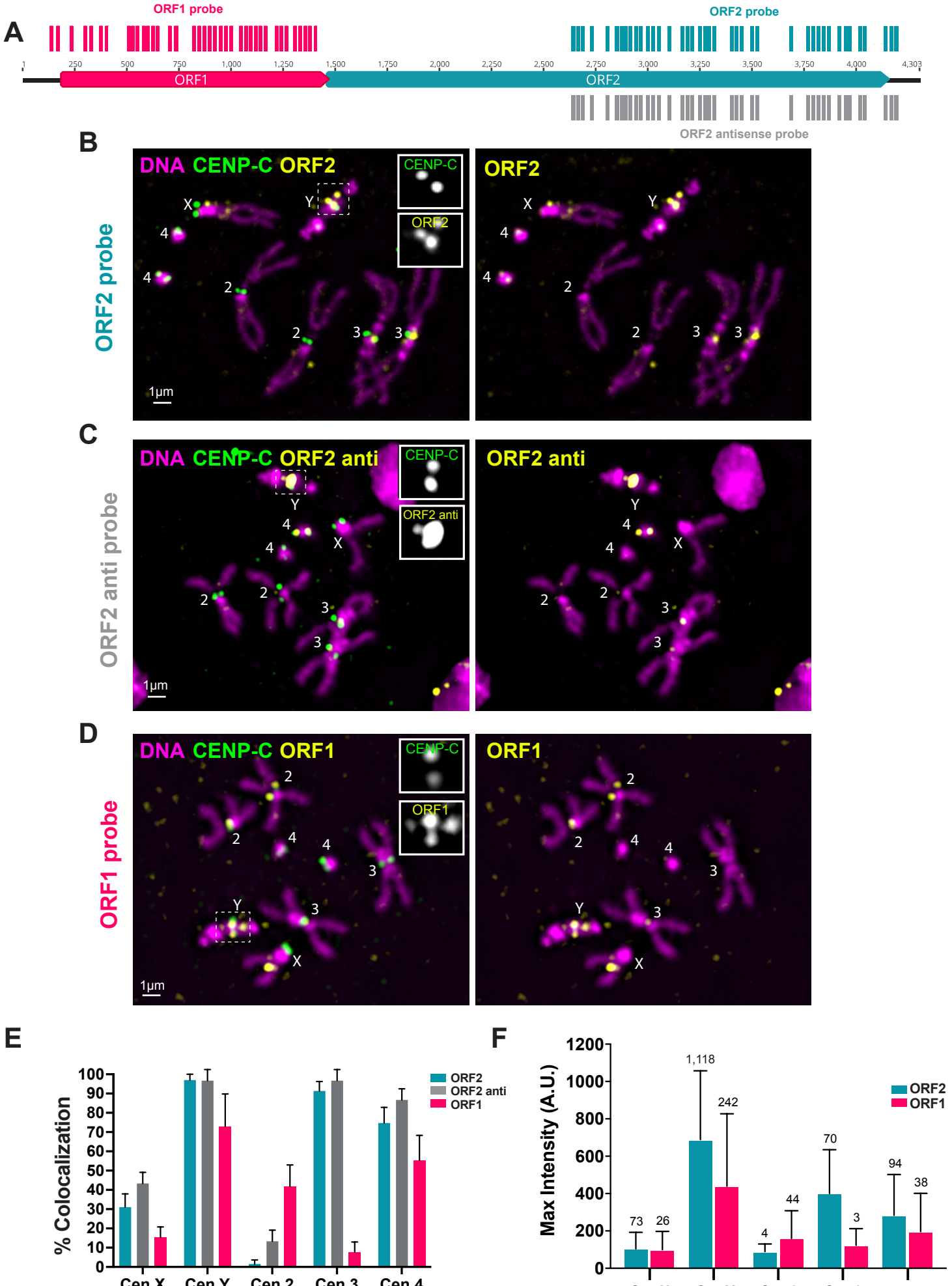
A
ORF1 probe
ORF2 probe
ORF1
ORF2
ORF2 antisense probe
B
ORF2 probe
DNA CENP-C ORF2
CENP-C
ORF2
ORF2
1µm
C
ORF2 anti probe
DNA CENP-C ORF2 anti
CENP-C
ORF2 anti
ORF2 anti
1µm
D
ORF1 probe
DNA CENP-C ORF1
CENP-C
ORF1
ORF1
1µm
E
% Colocalization
ORF2
ORF2 anti
ORF1
Cen X
Cen Y
Cen 2
Cen 3
Cen 4
F
Max Intensity (A.U.)
ORF2
ORF1
73
26
1,118
242
4
44
70
3
94
38
Cen X
Cen Y
Cen 2
Cen 3
Cen 4

Fig. 2

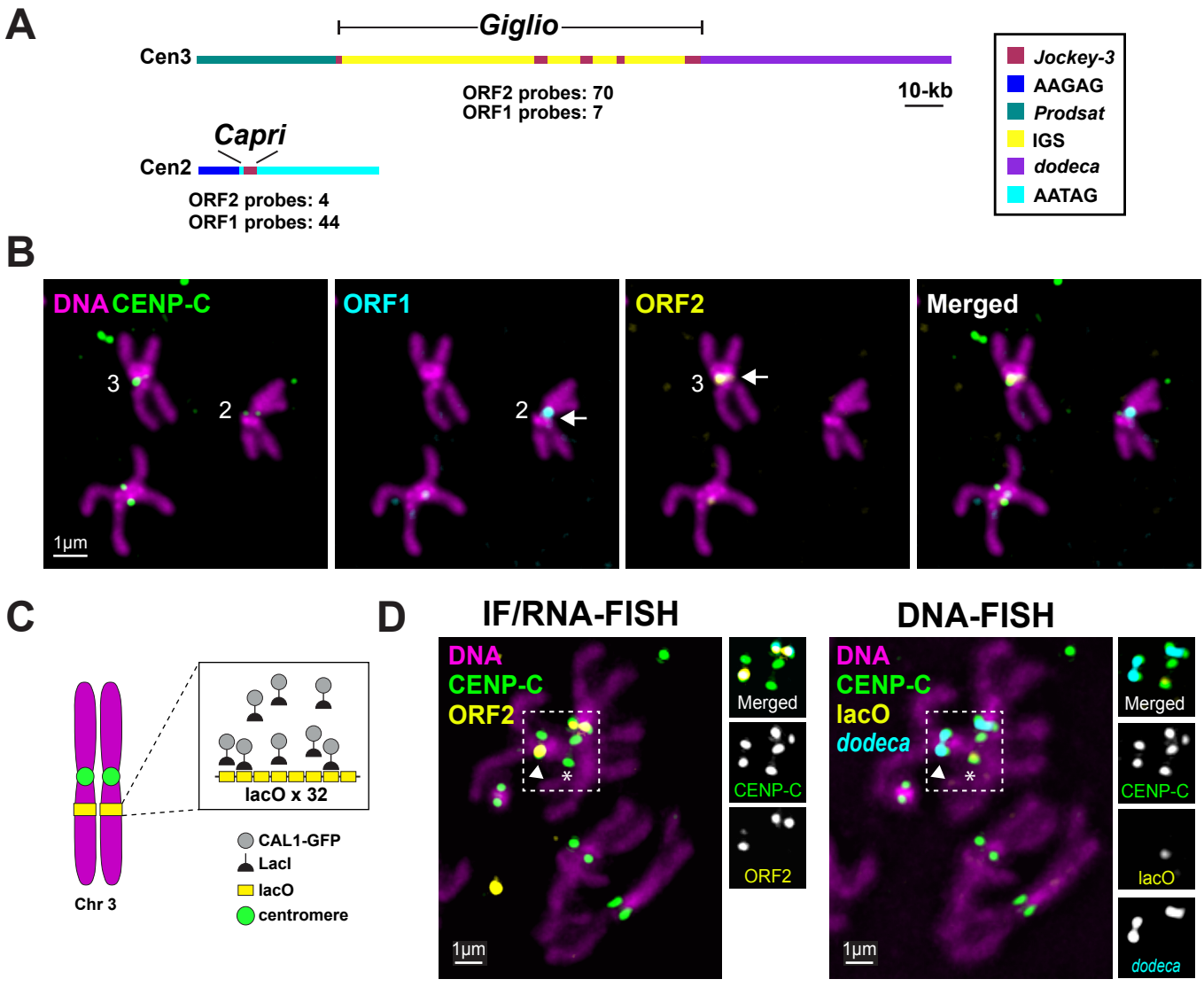
A
Giglio
Cen3
ORF2 probes: 70
ORF1 probes: 7
10-kb
Capri
Cen2
ORF2 probes: 4
ORF1 probes: 44
Jockey-3
AAGAG
Prodsat
IGS
dodeca
AATAG
B
DNA CENP-C
ORF1
ORF2
Merged
3
2
1µm
C
lacO x 32
CAL1-GFP
LacI
lacO
centromere
Chr 3
D
IF/RNA-FISH
DNA
CENP-C
ORF2
Merged
CENP-C
ORF2
1µm
DNA-FISH
DNA
CENP-C
lacO
dodeca
Merged
CENP-C
lacO
dodeca
1µm

Fig. 3

A

Location	CenX	CenY	Cen2	Cen3	Cen4	Total cen	Total non-cen	Total
Copies hit	2/21	31/147	0/2	2/11	4/21	39/202	41/127	80/329

B

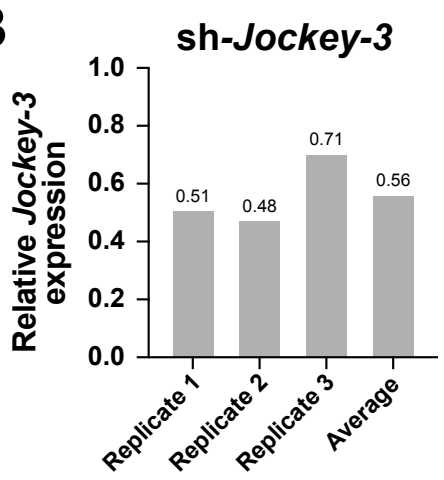

C

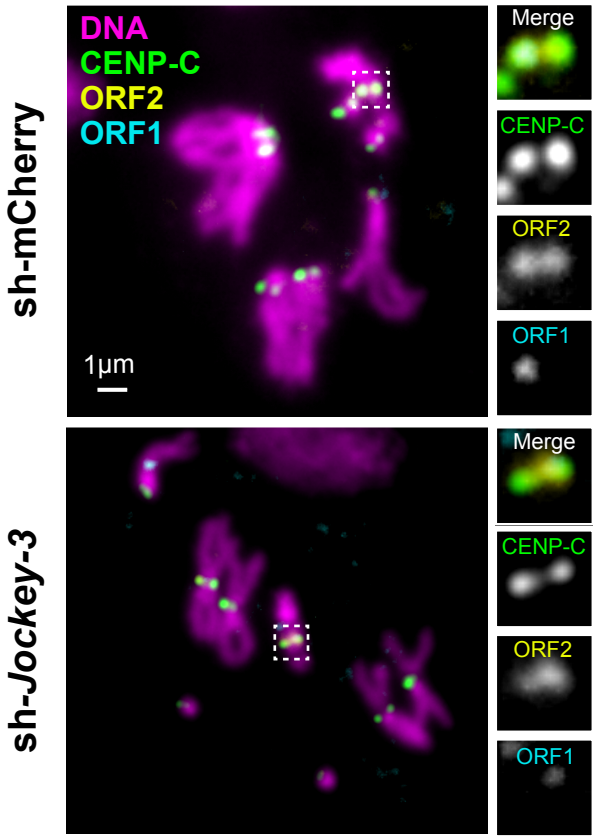

D

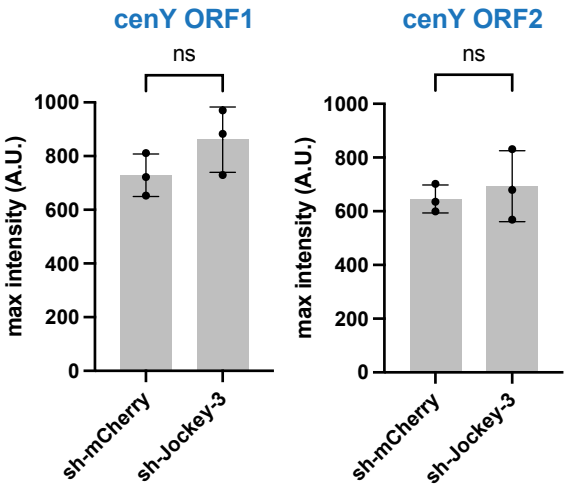

E

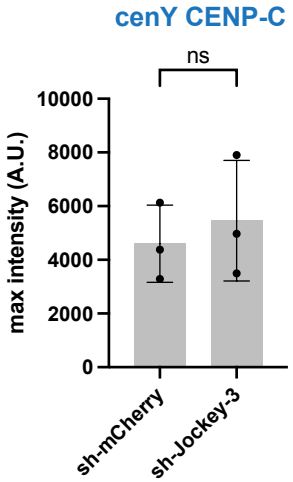

F

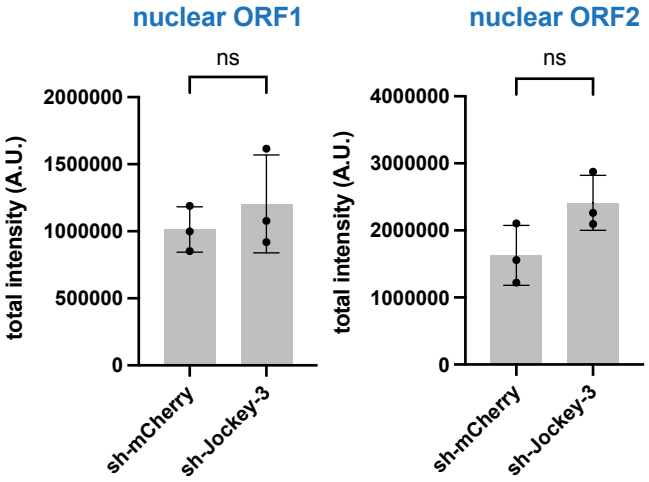

Fig. 4

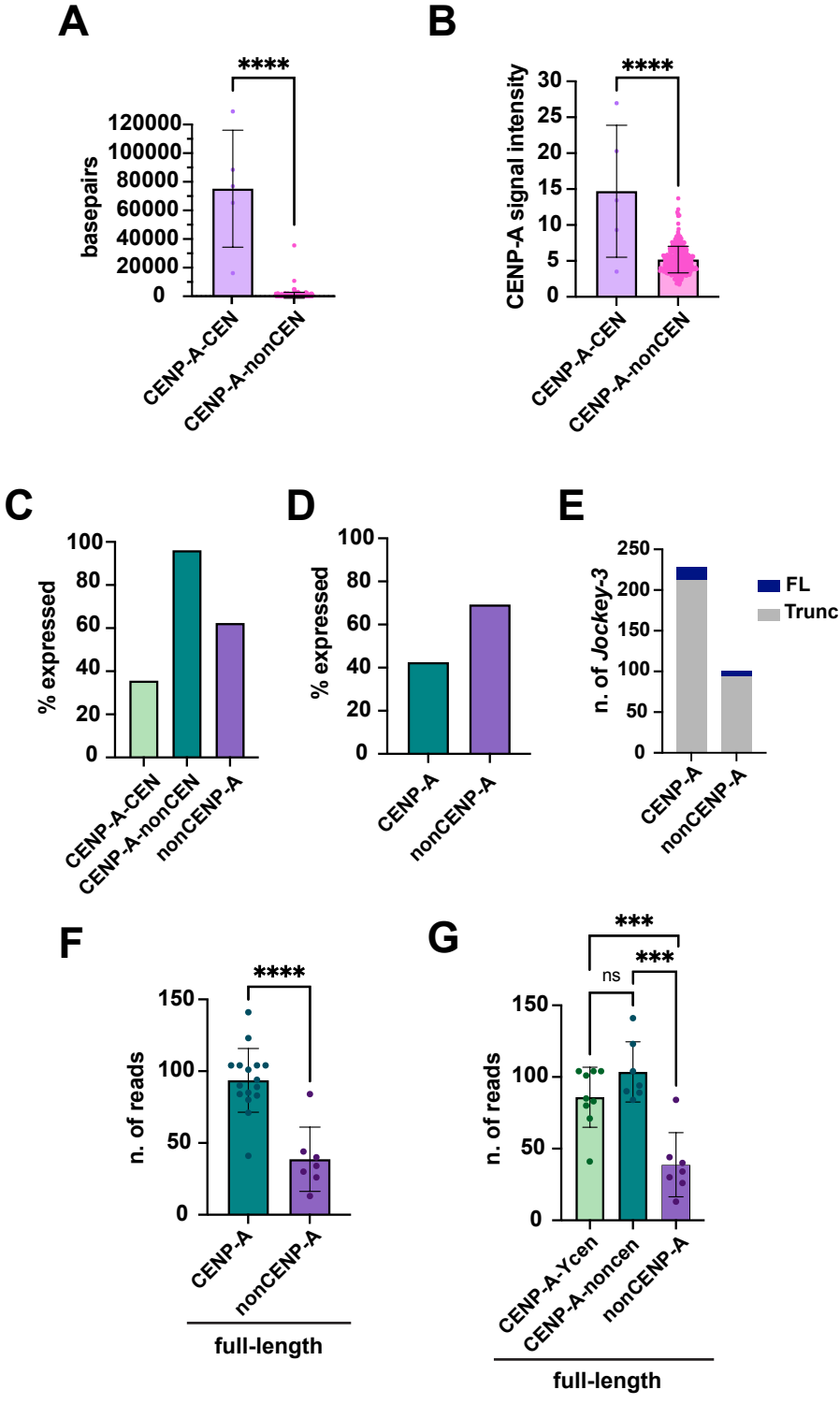
A
****
basepairs
120000
100000
80000
60000
40000
20000
0
CENP-A-CEN
CENP-A-nonCEN
B
****
CENP-A signal intensity
30
25
20
15
10
5
0
CENP-A-CEN
CENP-A-nonCEN
C
% expressed
100
80
60
40
20
0
CENP-A-CEN
CENP-A-nonCEN
nonCENP-A
D
% expressed
100
80
60
40
20
0
CENP-A
nonCENP-A
E
n. of Jockey-3
250
200
150
100
50
0
FL
Trunc
CENP-A
nonCENP-A
F
****
n. of reads
150
100
50
0
CENP-A
nonCENP-A
full-length
G
***
***
ns
n. of reads
150
100
50
0
CENP-A-Ycen
CENP-A-noncen
nonCENP-A
full-length

Fig. 5

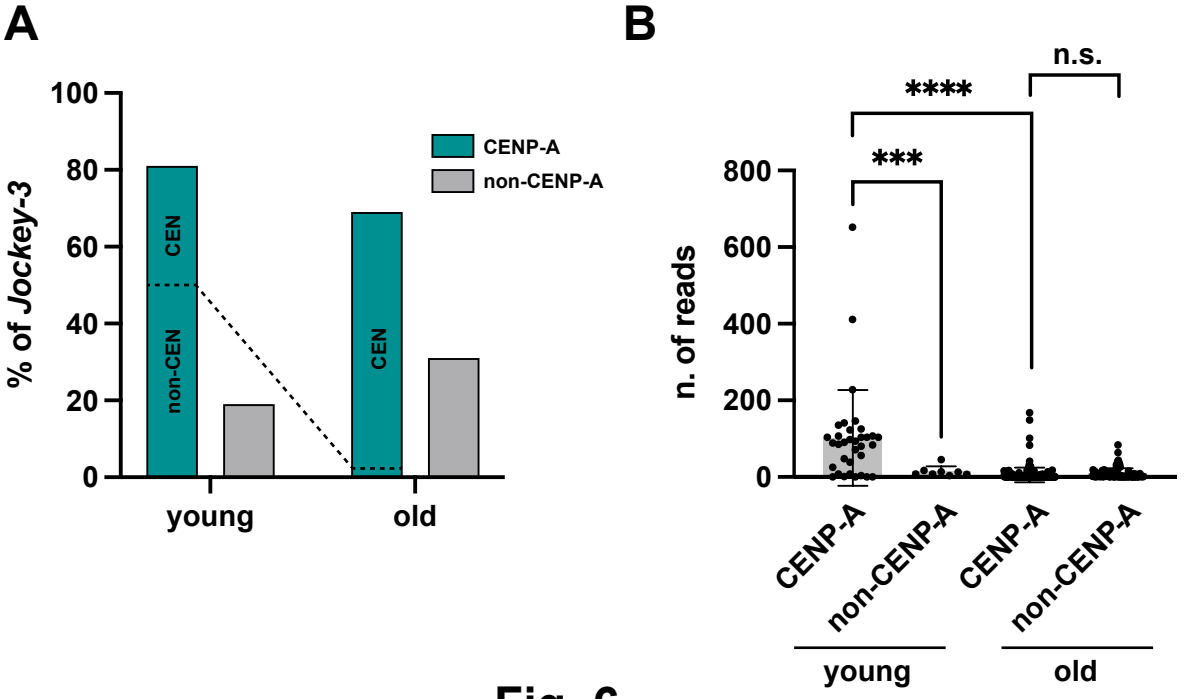
A
100
80
60
40
20
0
% of Jockey-3
CENP-A
non-CENP-A
CEN
non-CEN
CEN
young
old
B
n.s.
****
***
800
600
400
200
0
n. of reads
CENP-A
non-CENP-A
CENP-A
non-CENP-A
young
old

Fig. 6

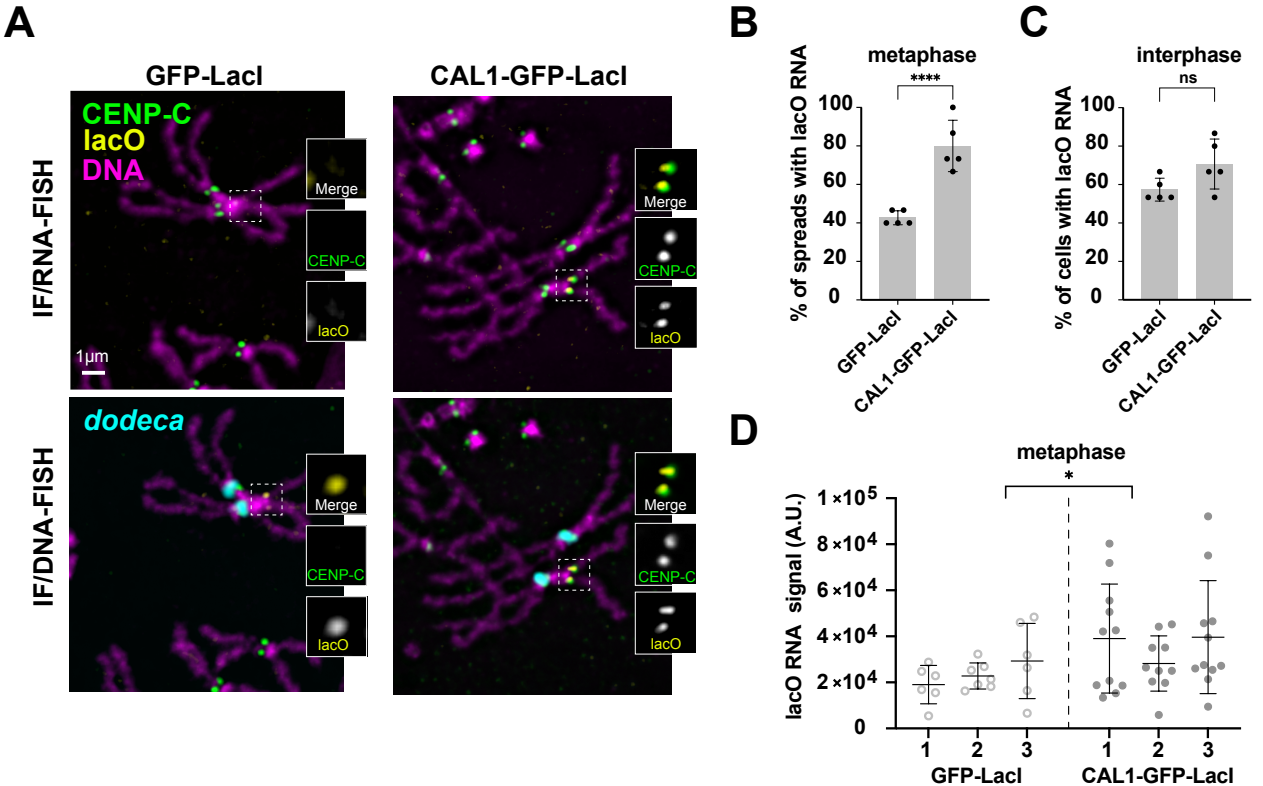
A
GFP-LacI
CAL1-GFP-LacI
CENP-C
lacO
DNA
IF/RNA-FISH
IF/DNA-FISH
dodeca
Merge
CENP-C
lacO
1µm
B
metaphase
****
% of spreads with lacO RNA
100
80
60
40
20
0
GFP-LacI
CAL1-GFP-LacI
C
interphase
ns
% of cells with lacO RNA
D
metaphase
*
lacO RNA signal (A.U.)
1×10^5
8×10^4
6×10^4
4×10^4
2×10^4
0
1
2
3
GFP-LacI
CAL1-GFP-LacI

Fig. 7